Bulletin of the Seismological Society of America, Vol. 92, No. 6, pp. 2186–2204, August 2002

Characteristics of the Ground Motion in Northeastern Italy

by Luca Malagnini, Aybige Akinci, Robert B. Herrmann, Nicola Alessandro Pino, and Laura Scognamiglio

Abstract A large data set of ground-velocity time histories from earthquakes that occurred in Friuli-Venezia Giulia (northeastern Italy) was used to define regional predictive relationships for ground motion, in the 0.25- to 14.0-Hz frequency band. The bulk of the data set was provided by the seismic network run by Centro Ricerche Sismologiche (CRS), a department of the Istituto Nazionale di Oceanografia e Geofisica (OGS). A collection of 17,238 selected recordings from 1753 earthquakes was compiled for the years 1995–1998, with magnitudes ranging from M_w ~1 to 5.6. Ninety-six three-component strong-motion waveforms belonging to the largest events of the 1976–1977 Friuli seismic sequence were also taken from the ENEA-ENEL accelerogram database and included in our data set. For the strongest event, which occurred on 6 May 1976 at 20:00 local time, an average local magnitude M_L 6.6 was computed by Bonamassa and Rovelli (1986). The inclusion of a large number of acceleration time histories from this earthquake and six others, from magnitudes from M_w 5.2 to magnitude M_s 6.1 (three of them of M_s ~6.0), extends the validity of the predictive relationships proposed in this study up to the highest magnitude ever recorded in the region.

A total of 10,256 vertical-component and 6982 horizontal-component seismograms were simultaneously regressed for excitation and site characteristics, as well as for the crustal propagation, in the hypocentral distance range 20–200 km. Results are given in terms of excitation, attenuation, and specific site for the vertical ground motion, together with a horizontal-to-vertical ratio for each existing horizontal-component seismometer. The regional propagation was modeled in the 0.5- to 14.0-Hz frequency band by using a frequency-dependent piece wise continuous linear (in a log–log space) geometrical spreading function and a frequency-dependent attenuation parameter:

$$Q(f) = 260(f/1.0)^{0.55}$$

The excitation spectra of larger events were modeled by using the regional propagation, a single-corner frequency Brune spectral model characterized by an effective stress parameter,

$$\Delta\sigma = 60 \text{ MPa},$$

and by a regional estimate of the near-surface, distance-independent, network-averaged attenuation parameter

$$\kappa_0 = 0.045 \text{ sec}$$

that was estimated from the rolloff of the empirical source spectra obtained from the regressions. Other studies (De Natale *et al.*, 1987; Cocco and Rovelli, 1989; Singh *et al.*, 2001) suggested large stress drops ($\Delta\sigma \simeq$ 30–100 MPa,) to explain the high-frequency amplitude levels of the seismic radiation of the largest quakes of the 1976 sequence.

Predictions for peak ground acceleration (PGA) and pseudo–spectral velocity (PSV) (5% damping) were computed through the use of the random vibration theory (RVT), with the parameters obtained from the regressions of this study.

Introduction

Large earthquakes that have occurred in recent years in densely populated areas of the world (Izmit, Turkey, 17 August 1999; Düzce, Turkey, 12 November 1999; Bhuj, India, 26 January 2001) dramatically highlighted the inadequacy of a massive portion of the buildings erected in and around the epicentral areas. The Izmit event was particularly destructive because a large number of buildings were unable to withstand even moderate levels of ground shaking, demonstrating poor construction criteria and, more generally, the inadequacy of the application of building codes for the region. Building earthquake-resistant structures and retrofitting old buildings on a national scale may be extremely costly and may represent an economic challenge even for developed western countries. Planning and design should be based on available national hazard maps, which, in turn, must be produced after a careful calibration of ground-motion predictive relationships (Kramer, 1996) for the region. Updating existing hazard maps represents one of the highest priorities for seismologists, both in terms of recomputing the ground motion and of reducing the related uncertainties. This important issue has been recently stressed by Cramer and Gomberg (2001), who also demonstrated the importance of quantitative predictions of the ground-motion parameters in the United States.

Predictive relationships are usually obtained using the classical approach of performing regressions on large numbers of strong-motion recordings (see Campbell and Bozorgnia, 1994 [for a worldwide study on peak horizontal accelerations]; Boore *et al.*, 1993 [for a study on western North America]; Ambraseys, 1995, Ambraseys *et al.*, 1996, Ambraseys and Simpson, 1996 [for their works on ground-motion scaling in Europe]; Sabetta and Pugliese, 1987, 1996 [for studies in the Italian region]). This approach has the disadvantage that there might be regions of high seismic potential that lack a significant number of observations, thus forcing the local adoption of perhaps inappropriate scaling relations. On the other hand, a number of articles have been published in the last few years on the determination of some aspects of ground-motion scaling in various regions of the world by exploiting the background seismicity. Chouet *et al.* (1978) suggested that the accurate determination of the scaling laws of small events was a promising way of estimating the strong motion in areas where past recordings from large earthquakes were unavailable.

Many studies have used weak-motion recordings for purposes of producing predictive relationships for the ground motion: Pino *et al.* (2001) worked on Greece and Crete; Akinci *et al.* (2001) worked on the region surrounding the city of Erzincan (eastern edge of the North Anatolian Fault Zone, [NAFZ], Turkey); more regions investigated with the same approach are the Apennines (Malagnini and Herrmann, 2000, Malagnini *et al.*, 2000a). Central Europe (Malagnini *et al.*, 2000b), Western Alps (Morasca *et al.*, 2002), Sicily (Scognamiglio *et al.*, 2001), Switzerland (Bay *et al.*, 2001), Utah (Jeon, 2000), Mexico (Ortega and Herrmann, 2000), the northwestern United States (Herrmann and Dutt, 1999), California (Raoof *et al.*, 1999), the central United States (Herrmann and Malagnini, 1996), and the Southern Great Basin (Samiezade-Yazd, 1993).

Relationships used by seismologists and engineers in Italy (including in the eastern Alps) are the ones calibrated over the Italian and European databases of strong ground motion recordings. Except the work by Chiaruttini and Siro (1981), who investigated the ground-motion scaling of northeastern Alps by using 120 horizontal-component, regional recordings from the 1976 Friuli earthquake sequence, other studies used very heterogeneous data sets. Chiaruttini and Siro (1981) defined a functional form to describe the decay of the peak horizontal acceleration (PHA) within 200 km of the source as a function of magnitude and distance. Specifically, Italian accelerogram time histories, gathered from events that occurred in different tectonic and geological environments (Friuli, Irpinia, and central Italy and Sicily) were used by Sabetta and Pugliese (1987, 1996), who investigated the attenuation with epicentral distance of peak ground acceleration (PGA), peak ground velocity (PGV), and response spectra. Sabetta and Pugliese carried out a series of regressions on peak amplitudes by using a functional form that did not consider anelastic energy losses but described the dependence on distance only in terms of a constant geometrical spreading at all distances ($g(r) = 1/r$).

Ambraseys and coworkers used the European database of strong ground motion recordings (accelerograms) to provide a set of relationships for peak values and response spectra. Ambraseys and Bommer (1991) produced predictive relationships for horizontal and vertical PGA in Europe, using 529 three-component strong-motion records generated by 219 shallow earthquakes in the European region, mostly taken from the Alpide Belt. Data were chosen from the 1991 European Earthquake Strong Motion Database using the following criteria: $M > 4.0$ and focal depth no greater than 25 km. The Italian data set used by Sabetta and Pugliese (1987) was also included. Ambraseys and Bommer (1991) observed that the mean vertical-to-horizontal ratio of peak acceleration was almost independent of magnitude and distance and equal to 0.5. No site geology was taken into account during their regressions. As a rule-of-thumb regarding the vertical-to-horizontal ratio of the PGA, Newmark and Hall (1982) proposed a value of two-thirds. Ambraseys *et al.* (1996) reevaluated their previous predictive relationship for horizontal acceleration using a larger data set, and Ambraseys and Douglas (2000) provided similar models from a data set of near-field acceleration time histories.

In the present study we regress the peak values of narrow bandpass-filtered ground velocity time histories and root mean square (rms) average Fourier spectral amplitudes at a set of frequencies in order to define (1) an attenuation function made of a piecewise linear geometrical spreading (in

log–log space) and a frequency-dependent crustal $Q(f)$ and (2) an excitation function containing the competing effects of high-frequency terms: an effective stress parameter, $\Delta\sigma$, and a high-frequency attenuation term $\exp(-\pi\kappa_0 f)$. These parameters, together with the information on the effective duration of the ground motion in the region, as a function of distance and frequency, are used to obtain estimates of the peak ground motion (PGA, PGV) and response spectra (5% damping). The code used for these calculations was stochastic model simulation (SMSIM) by Boore (1996). We compared, when possible, our results with those by other authors who worked in the region.

This work is part of a larger effort, supported by the Istituto Nazionale di Geofisica e Vulcanologia of Rome (INGV), through the project "Terremoti probabili in Italia tra l'anno 2000 e il 2030: elementi per la definizione di priorità degli interventi di riduzione del rischio sismico," task 3.1 by the Gruppo Nazionale Difesa dai Terremoti (GNDT) and the project "Progetto triennale per la valutazione delle leggi di attenuazione nei paesi della regione mediterranea," supported by INGV for the systematic investigation of the crustal attenuation within the Mediterranean region. The ultimate goals of the two projects are the production of modern hazard maps at the Italian and Mediterranean scales, respectively, based on the use of predictive relationships estimated regionally.

Seismotectonics of Friuli

Friuli is a region of northeastern Italy, at the boundary with Austria and Slovenia. The area is mostly covered by the eastern part of the Southalpine Chain and is characterized by the interaction of two mountain belts, the Dinarides and the Southern Alps. The Northeastern part of Italy has significant seismic activity, with several destructive historical earthquakes, especially in the Veneto and Friuli regions, where the contact between the two chains, the Southern Alps and Dinarides (on the eastern side of the Adriatic Sea), occurs (Slejko, 1987; Carulli *et al.*, 1990). Current seismic activity has been recorded since 1977 by a local seismic network of the Istituto Nazionale di Oceanografia e Geofisica Sperimentale, which monitors the entire region. The majority of hypocenters in the active area in central Friuli have depths between 7.5 and 11 km, whereas those in the eastern part have depths down to about 20 km (Slejko, 1987). In the western part of Friuli, the depth distribution is clustered with a maximum density between 7.5 and 13.5 km (Bressan *et al.*, 1998). Different focal mechanisms have been proposed for the seismic sequence that started in May 1976 with a mainshock of m_b 6.2 (PDE catalog) (6 May 1976: CMT Harvard-estimated M_w 6.5), although they can generally be interpreted as showing northward-dipping thrust motion with a small dextral E–W strike-slip component (Pondrelli *et al.*, 2001). The compressive style remains well defined in the Alps, whereas toward the east the available focal mechanisms generally show strike-slip patterns in Veneto and Austria, and vertical movement along the Sava line, Slovenia (Slejko *et al.*, 1989).

Figure 1 shows the geologic and tectonic features described in this section. Both reflect in shape and in geodynamic evolution the collision between the Adria microplate and the European plate (Carulli *et al.*, 1990; Braitenberg, 2000). Along the Southalpine Chain, the Friulian Alps experienced the greatest shortening and are characterized by the strongest seismicity (Bressan *et al.*, 1998). The stratigraphic sequence involved in the Alpine orogeny of this sector of the chain is about 14 km thick (Selli, 1963; Spalletta and Venturini, 1989), a depth that contains most of the background seismicity in Friuli.

The Eastern Alps have been investigated by several deep seismic soundings (DSS) campaigns (e.g., Giese and Prodehl, 1976; Gebrande *et al.*, 1978; Aric *et al.*, 1987; Slejko, 1987, [and references therein]). From Istria (south of Trieste) northward, the Moho deepens smoothly, attaining a depth of 40 km after a pronounced flexure below the Southern Alps front (Slejko *et al.*, 1989; Carulli *et al.*, 1990), and a seismic layer with velocity values close to 6.7 km/sec has been found at a depth of about 10 km in central Friuli.

The Friuli–Venezia Giulia Seismic Network (FVGSN)

At the end of 1998, the Friuli–Venezia Giulia Seismic Network (FVGSN) was composed of 15 digital seismic stations: five of them (BAD, BOO, CAE, DRE, ZOU) were equipped with three-component seismometers, whereas the remaining 10 sites (BUA, COLI, CSM, CSO, LSR, MLN, MPRI, PLRO, TLI, UDI) were instrumented with single-component, vertical seismometers. Between the end of 1998 and the beginning of 2002, more stations were added to the network, and additional horizontal-component seismometers integrated with some of the single-component stations. Figure 2 shows the locations of the stations and of the recorded events. One additional station of the FVGSN (TRI), which belongs to Med-Net, is equipped with very broadband instruments (not used in this study). The FVGSN is run by the Centro di Ricerche Sismologiche (CRS), located in Udine. The CRS is a department of the former Osservatorio Geofisico Sperimentale (OGS), now Istituto Nazionale di Oceanografia e Geofisica Sperimentale. The network is funded by the Regione Friuli–Venezia Giulia through its Civil Defense Agency. Data collected by FVGSN are directly accessible at *http://bbtri.ogs.trieste.it/*.

Until the end of 1998, 9 of the 15 stations in Friuli (BOO, BUA, CSM, COLI, CSO, LSR, MPRI, PLRO, MLN) were equipped with Willmore MKIIIA 1-Hz vertical seismometers; four sites (BAD, CAE, DRE, ZOU) were instrumented with 1-Hz, three-component seismometers (Lennartz LE-3D). Station UDI is equipped with a Kinemetrics FBA-23, three-component accelerometer; and TLI is equipped with a vertical borehole seismometer, installed at a depth of about 100 m. BAD has also a Kinemetrics "Episensor" accelerometer. Data recorded from local Lennartz MARS88

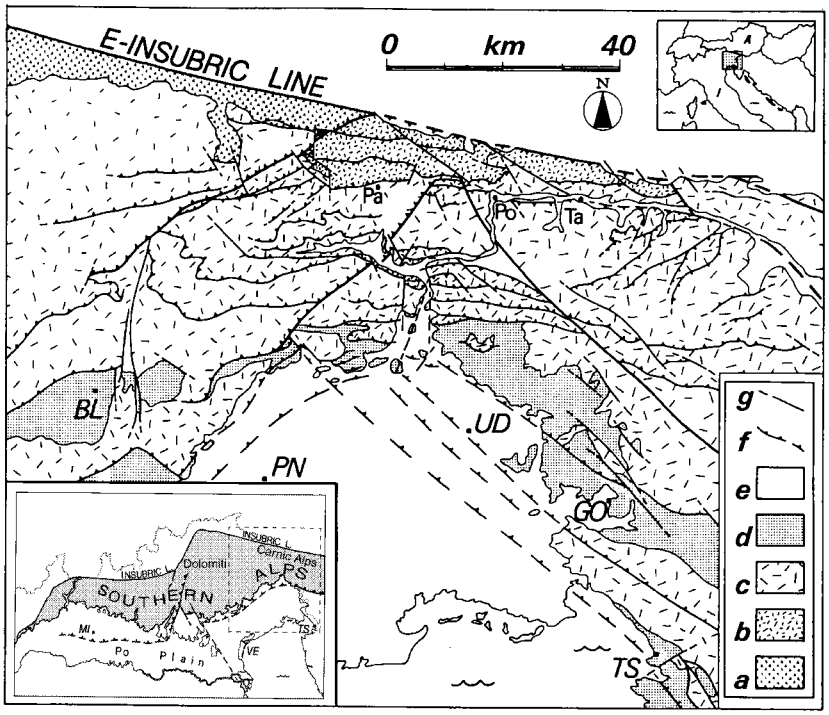

Figure 1. Schematic geologic map of the eastern Southern Alps (modified from Bressan *et al.*, 1998): a, Hercynian low metamorphic basement (Ordovician–Carboniferous); b, Paleocarnic nonmetamorphic Chain (Upper Ordovician-Carboniferous) and Upper Carboniferous-Lower Permian covers; c, Permo-Mesozoic mainly carbonatic successions; d, Flysch (Upper Mastrichtian-middle Eocene) and molassic sequence (Miocene); e, Quaternary alluvial deposits and moraines; f, thrust; g, subvertical fault; BL, Belluno; PN, Pordenone; UD, Udine; GO, Gorizia; TS, Trieste; Pa, Paluzza; Po, Pontebba; Ta, Tarvisio; MI, Milan; VE, Venice.

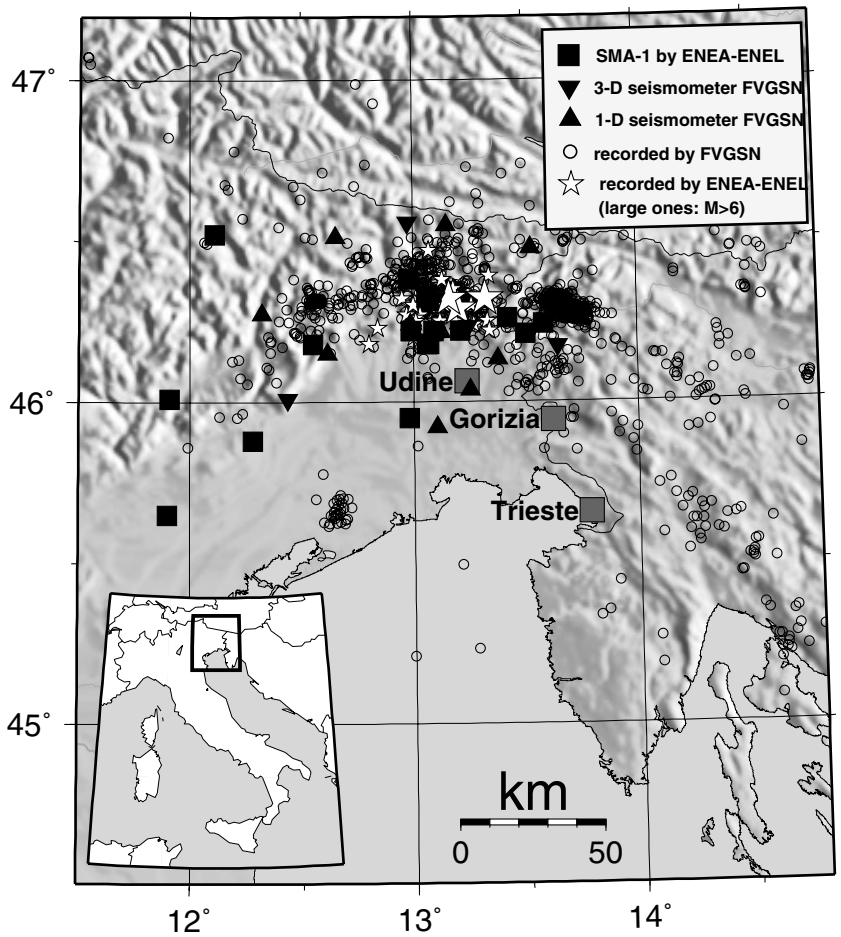

Figure 2. Map of the region: the locations of the seismometers of the FVGSN and the ENEA-ENEL accelerometer networks used in this study are indicated by triangles and squares, respectively. The epicentral locations of the events from the background seismicity recorded by the FVGSN for the years 1995–1998 are indicated by open circles, whereas stars mark the locations of the large events recorded by the ENEA-ENEL SMA-1 accelerometers in 1976–1977. Larger stars refer to events with $M_s \geq 6.0$.

systems are radiotelemetred to Udine for recording by the central MARS88/RC unit. MARS88 digitizers are used locally with STA/LTA triggering procedures. The sampling rate is set to 16×10^{-3} sec, and the dynamic range is 120 dB. Absolute time is provided by DCF signal. Table 1 (from Istituto Nazionale di Oceanografia e Geofisica Sperimentale [OGS], 2000) provides all the information about the FVGSN sites.

In addition to the stations of the FVGSN, analog strong-motion recordings of the 1976–1977 sequence from the ENEA-ENEL network were also integrated into the data set. The ENEA-ENEL network was equipped with SMA-1 accelerometers. Information about the ENEA-ENEL stations used in this study is given in Table 2.

The Data Set

The data set analyzed in this study consists of 1753 selected earthquakes recorded by the digital network during the years 1995–1998, in the magnitude range of M_w 1.0–5.6. Accelerograms from 29 events of the 1976 seismic sequence (M_{Lmax} 6.5), recorded by the accelerograph network run by the National Power Agency (ENEL), were added to the data base after being corrected for the instrument response and integrated to ground velocity. The 1976–1977 sequence was of particular interest, because it was characterized by a series of events of comparable sizes.

The integrated data set results in 10,256 vertical and in 6982 horizontal seismograms. Figure 3 depicts the spatial distribution of the vertical recordings with respect to the hypocentral distance for each station in the FVGSN network (ZOU, UDI, TLI, PLRO, MPRI, MLN, LSR, DRE, CSO, CSM, COLI, CAE, BUA, BOO, BAD), as well as for stations of the ENEA-ENEL accelerograph network. From a visual inspection of Figure 3 (vertical-component seismograms) we note that the spatial sampling of the available recordings is extremely dense and well distributed, at least out to a 200-km hypocentral distance. This characteristic leads to excellent regression results. Figure 4 similarly describes the distance distribution of the horizontal recordings. More information about the distribution of the events and the recordings of our data set with hypocentral depth, magnitude, and hypocentral distance are given in Figure 5.

Data Processing

As a first step in the processing, we corrected all the seismograms for the instrument response, obtaining ground velocity in units of m/sec. Regressions were carried out separately on peak values of filtered ground velocity and on Fourier spectral amplitudes at the same set of selected central frequencies $\{f_{cl}\}$. A bandpass filter at f_{cl} is built as the combination of two causal 8-pole butterworth filters: a low-pass filter with corner at $\sqrt{2}f_{cl}$, and a high-pass filter with corner at $1/\sqrt{2}f_{cl}$.

The kth seismogram, for the ith event at the jth station, is passed through the bandpass filter around f_{cl}, and the logarithm of its peak value is written as the sum of an excitation term relative to an arbitrary reference distance, a site term, and a propagation term:

$$A_k(f_{cl}, r_{ij}) = \mathrm{EXCIT}_i(f_{cl}, r_{ref}) + \mathrm{SITE}_j(f_{cl}) + D(r_{ij}, r_{ref}, f_{cl}). \quad (1)$$

We chose the following set of central frequencies: (f_{cl} = 0.25, 0.3, 0.4, 0.5, 1.0, 2.0, 3.0, 4.0, 5.0, 6.0, 8.0, 10.0, 12.0, and 14.0 Hz). During the regressions, the degrees of freedom of the system are reduced and stability is introduced by imposing the following constraints:

Table 1
Some Information on the FVGSN Stations

Station	Lat. (N)	Long. (E)	Elevation (m above sea level)	Geology	Start of Operation	Sensor
BAD	46.234	13.243	590	limestone	6 May 1977	LE-3D Lite + FBA-23
BOO	46.320	13.099	444	limestone	9 May 1977	MKIII + Episensor
BUA	46.217	13.124	320	flysch	6 May 1977	MKIII
CAE*	46.009	12.438	870	limestone	23 April 1983	MKIII
COLI	46.132	13.377	250	flysch	6 May 1977	MKIII
CSM*	46.512	12.652	1640	flysch	6 May 1977	MKIII
CSO*	46.273	12.324	1070	limestone	1 January 1988	MKIII
DRE	46.173	13.644	810	marly Sandstone and fract. limestone	20 December 1982	LE-3D
LSR	46.475	13.527	1750	porphyry, diabase spilite	1 January 1988	MKIII
MLN*	46.150	12.616	814	limestone	14 November 1985	MKIII
MPRI	46.241	12.987	762	limestone	20 June 1977	MKIII
PLRO	46.549	13.148	1420	diabasi	1 January 1988	MKIII
TLI	45.921	13.103	74	alluvium	27 November 1985	L4C
UDI	46.037	13.253	90	gravels	24 June 1977	FBA-23
ZOU	46.557	12.974	1896	dolomite	17 October 1982	LE-3D Lite

*Stations where duration is characterized by a bilinear distribution at large hypocentral distances ($r > 50$–70 km; see Fig. 7). These systematic behaviors are not obviously related to site geology (e.g., alluvium versus hard-rock sites).

Table 2
Some Information on the ENEA-ENEL Accelerograph Stations Used in the Regressions Described in This Study

Station	Lat. (N)	Long. (E)	Elevation (m)	Geology	Sensor
Barcis	4.618000e+01	1.255000e+01	420	thin-alluvium site (soft)	SMA-1
Forgaria	4.622000e+01	1.299000e+01	205	thin-alluvium site (soft)	SMA-1
Tarcento	4.622000e+01	1.321000e+01	230	thin-alluvium site (soft)	SMA-1
Tolmezzo	4.638000e+01	1.298000e+01	525	thin-alluvium site (soft)	SMA-1
Castelfranco	4.565000e+01	1.190000e+01	42	thick-alluvium site (stiff)	SMA-1
Codroipo	4.595000e+01	1.298000e+01	30	thick-alluvium site (stiff)	SMA-1
Conegliano	4.588000e+01	1.228000e+01	65	thick-alluvium site (stiff)	SMA-1
Asiago	4.585000e+01	1.147000e+01	975	rock site	SMA-1
Feltre	4.601000e+01	1.191000e+01	320	rock site	SMA-1
Malcesine	4.581000e+01	1.085000e+01	95	rock site	SMA-1
Monselice	4.525000e+01	1.172000e+01	10	rock site	SMA-1
San Rocco	4.622000e+01	1.299000e+01	405	rock site	SMA-1
Somplago	4.633000e+01	1.306000e+01	198	rock site	SMA-1
MaiMunic	4.618000e+01	1.307000e+01	168	thick-alluvium site (stiff)	SMA-1
MaiPiano	4.618000e+01	1.306000e+01	168	thick-alluvium site (stiff)	SMA-1
Cortina	4.652000e+01	1.211000e+01	1550	rock site	SMA-1
Tregnago	4.552000e+01	1.113000e+01	500	rock site	SMA-1
MaiPrato	4.618000e+01	1.306000e+01	169	thick-alluvium site (stiff)	SMA-1
Robic	4.621000e+01	1.350000e+01	N/A	rock site	SMA-1
Kobarid	4.624000e+01	1.358000e+01	N/A	thin-alluvium site (soft)	SMA-1
Buia	4.622000e+01	1.309000e+01	N/A	thin-alluvium site (soft)	SMA-1
Breginj	4.626000e+01	1.342000e+01	N/A	thick-alluvium site (stiff)	SMA-1

Data from these stations are not used to define duration functions of Figure 7.

(1) the propagation term is normalized to zero at an arbitrary reference distance:

$$D(r = r_{\text{ref}}, f) = 0, \tag{2}$$

and

(2) the sum of the site terms at all the available vertical sites is forced to be zero. Horizontal site terms are left free to vary. Moreover, stations affected by local effects (determined after trial runs) are set free to vary during the regressions.

The propagation term is parameterized as a piecewise linear function with numerous nodes, and a linear interpolation is taken between adjacent nodes. A further constraint of minimum roughness is forced on the crustal attenuation function $D(r, r_{\text{ref}}, f)$. At the end of this process, we cast all our data into a large matrix form and invert for excitation, site, and propagation terms.

The importance and implication of constraint 2 are that it does not only stabilize the regression, but it also gives a precise physical meaning to all our results. More explicitly, constraint 2 forces some of the inverted quantities (propagation and excitation terms) to be referred to vertical motion. Horizontal ground motion is implicitly supposed to decay with distance the same way as the vertical motion does.

Fourier amplitudes are processed by using a slightly more complicated, three-step preprocessing procedure. First, the instrument-corrected seismogram is passed through the bandpass-filter centered on the lth frequency, f_{cl}, and the duration of the filtered signal that follows the S-wave onset (T) is quantified. Second, we go back to the original seismogram and compute the Fourier amplitude spectrum on the time window of length T that starts at the S-wave onset. Third, the Fourier amplitude spectrum is rms averaged between the corners used to define the corresponding bandpass filter, $0.707\, f_{\text{cl}}$ and $1.414\, f_{\text{cl}}$. This rms average is taken as our observation of the amplitude spectrum $A_{ij}(f_{\text{cl}}, r_{ij})$. Equation (1) is used to describe each observation and to cast each one into a matrix form to be used for a simultaneous inversion of excitation, site, and propagation quantities. The rms average is used in the regression only if the observed peak of the corresponding filtered time history lies within a standard deviation from a predicted peak value obtained through RVT (see the presentation by Cartwright and Longuet-Higgins, 1956). In both cases (peak filtered velocities and Fourier amplitudes), data are processed separately at each sampling frequency.

As an improvement on previous studies, we decided to implement a faster and more effective L_1-norm inversion scheme (Bartels and Conn, 1980) for all the steps of the regressions. The L_1-norm algorithm is much less sensitive to large outliers than a classic least-squares one, even though for the evaluation of the standard errors we still compute the L_2 solution because no such objects are defined in the L_1-norm statistics.

Results

Duration of Ground Motion

In our study, duration as a function of hypocentral distance and frequency is used for the computation of peak

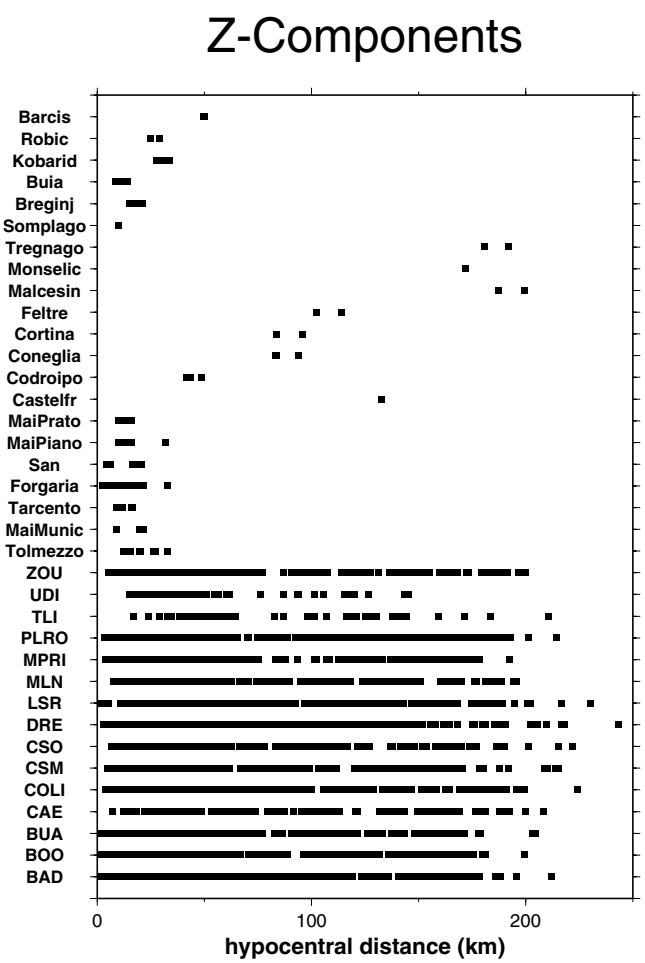

Figure 3. Source-receiver distance distributions of the vertical-component data set used in this study for each of the 21 ENEA-ENEL accelerometers (upper) and 15 FVGSN seismometers (lower) The horizontal axis refers to hypocentral distance (km). Each black square in the figure represents a single vertical-component seismogram recorded by the corresponding station (vertical component). The strong-motion observations do not contribute to the distance dependence because of their sparse number. Their excitation uses the distance dependence defined by the background seismicity determined by the FVGSN.

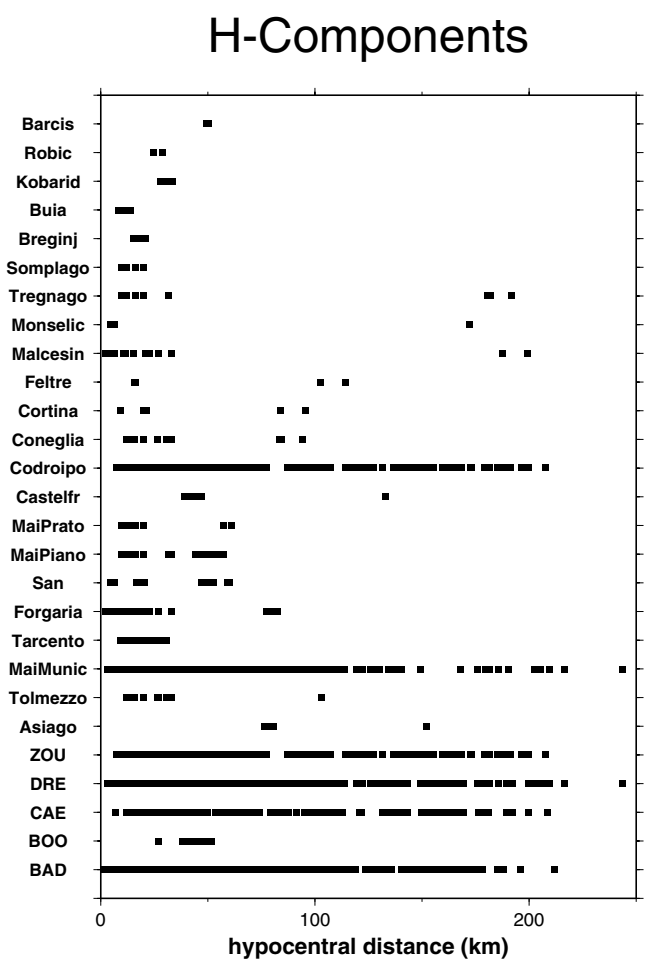

Figure 4. Same as Figure 3, for horizontal-component seismograms. Note that only five stations from FVGSN are included in the figure; since the Asiago accelerometer contributes to the horizontal-component data set, the number of ENEA-ENEL accelerograph stations in this Figure is now 22. Note that even though most of the ENEA-ENEL instruments recorded events in the 0- to 80-km range, the stations Codroipo, MaiMunic, and to some extent Asiago, nicely sample the hypocentral distance range: 0–200 km. The five three-component sites from FVGSN evenly sample the indicated hypocentral distance range. As explained in Figure 3, integrated acceleration data are used only to compute excitation terms at the largest magnitudes, whereas the regional attenuation term is evaluated only on weak-motion recordings from the FVGSN.

amplitudes and response spectra through RVT. Duration is the result of two distinct processes: dispersion and fault rupture. Dispersion is defined by scattering and wave propagation through an inhomogeneous, attenuating medium, and the duration of fault rupture depends on fault dimensions, rupture velocity, and geometry.

As defined in previous studies (e.g., Raoof *et al.*, 1999; Malagnini *et al*, 2000a,b; Malagnini and Herrmann, 2000), the duration at the frequency f_{cl} is calculated as the length of the time window (T) that brackets 5%–75% of the integral of the seismic energy computed on the filtered time history at that frequency (Fig. 6). The distribution of the calculated durations on each vertical and horizontal seismogram, (essentially, duration due only to the dispersion process) is given in Figure 7, at the central frequencies: 1.0, 2.0, 4.0, 8.0, 10.0, and 14.0 Hz.

Note that the individual durations shown in Figure 7 are bimodally distributed for distances larger than 50–70 km. The bulk of the observations follows the duration that is indicated by the lines connecting the diamonds, whereas a minority of duration points follow a different trend, indicating much longer durations (energy reverberations) at large distances.

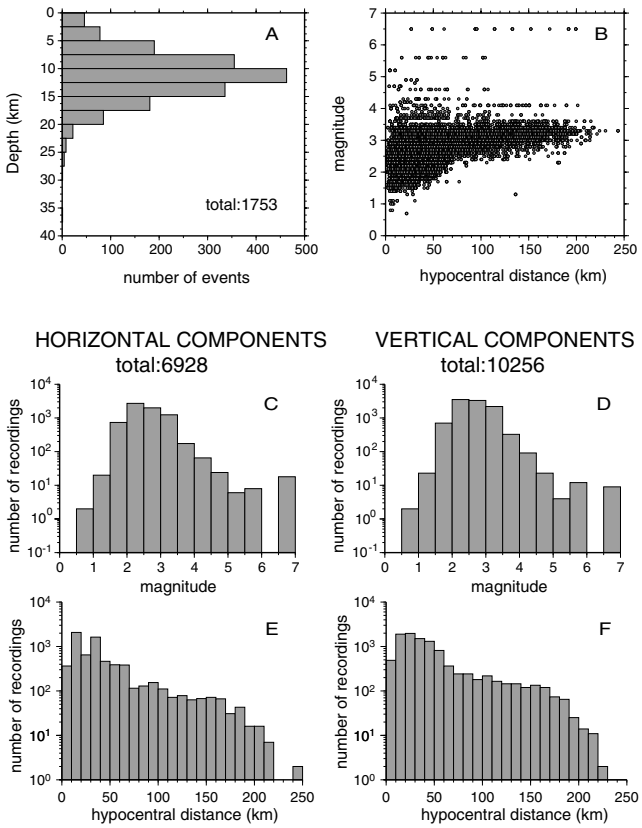

Figure 5. The figure describes the characteristics of the seismicity included in the integrated database of the FVGSN and ENEA-ENEL waveforms. (A) Distribution of the recorded events with respect to hypocentral depth; (B) distribution of magnitudes with respect to hypocentral distance; (C) number of horizontal recordings as a function of magnitude; (D) same as C, but for the vertical recordings; (E) number of horizontal recordings as a function of hypocentral distance; (F) same as E, but for vertical recordings.

We investigated the bimodal character of the individual distributions, where the high-frequency data sets show a clear second branch at large distances. Although the maximum variability between the site term amplitudes is well over a log unit, the analysis of the site terms defined by the regressions (shown below) does not show any outstanding site amplification due to the shallow geology that may be correlated with long durations. Asterisks by station names in Table 1 indicate stations where duration is characterized by a bilinear distribution at large hypocentral distances ($r >$ 50 − 70 km) (see Fig. 7). We see that there is no obvious relation to site geology (e.g., alluvium versus hard-rock sites).

Vertical Motion Crustal Attenuation

The crustal attenuation term, $D(r, r_{\text{ref}}, f)$, empirically determined for PGVs and Fourier amplitudes at each central frequency, is shown in Figure 8 (curves in color). In the

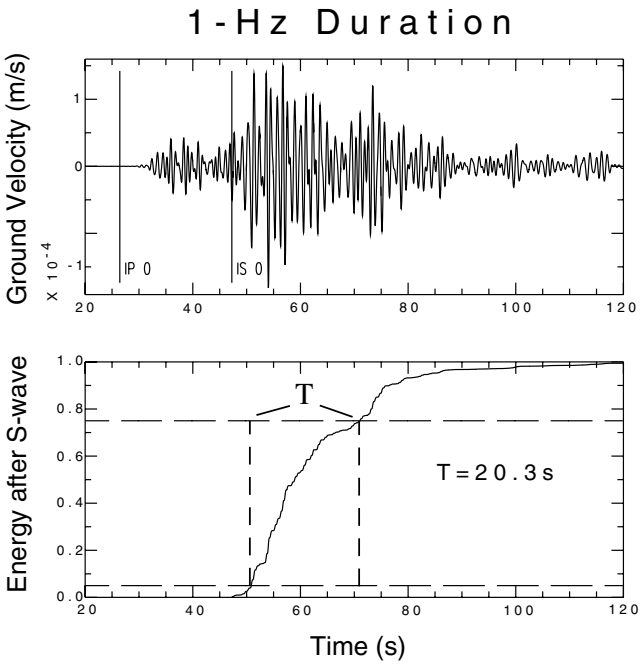

Figure 6. The process of estimating duration at the central frequency of 1.0 Hz is visually described. The integrated energy is normalized to a unit asymptotic plateau.

background of each frame, a set of smoother curves in black represents theoretical predictions at the same set of frequencies, obtained through the functional form:

$$D(r, r_{\text{ref}}, f) = \log g(r) - \log g(r_{\text{ref}}) - \frac{\pi f(r - r_{\text{ref}})}{\beta Q_0 (f/f_{\text{ref}})^{\eta}} \log e, f_{\text{ref}} = 1.0 \text{ Hz}; r_{\text{ref}} = 40 \text{ km}. \quad (3)$$

Best fit in the 0.5- to 14.0-Hz frequency band is obtained using the following frequency dependent attenuation parameter:

$$Q(f) = 260(f/1.0)^{0.55}, \quad (4)$$

together with a slightly frequency-dependent geometrical spreading:

$$g(r)|f_{\text{cl}} \le 1.0 \text{ Hz} = \begin{cases} r^{-1.0} & r \le 50 \text{ km} \\ r^{-1.6} & 50 < r \le 60 \text{ km} \\ r^{-1.2} & 60 < r \le 80 \text{ km} \\ r^{-1.3} & 80 < r \le 100 \text{ km} \\ r^{-0.5} & r > 100 \text{ km} \end{cases} \quad (5a)$$

$$g(r)|f_{\text{cl}} > 1.0 \text{ Hz} = \begin{cases} r^{-0.95} & r \le 40 \text{ km} \\ r^{-1.2} & 40 < r \le 50 \text{ km} \\ r^{-1.8} & 50 < r \le 60 \text{ km} \\ r^{-1.2} & 60 < r \le 100 \text{ km} \\ r^{-0.5} & r > 100 \text{ km}. \end{cases} \quad (5b)$$

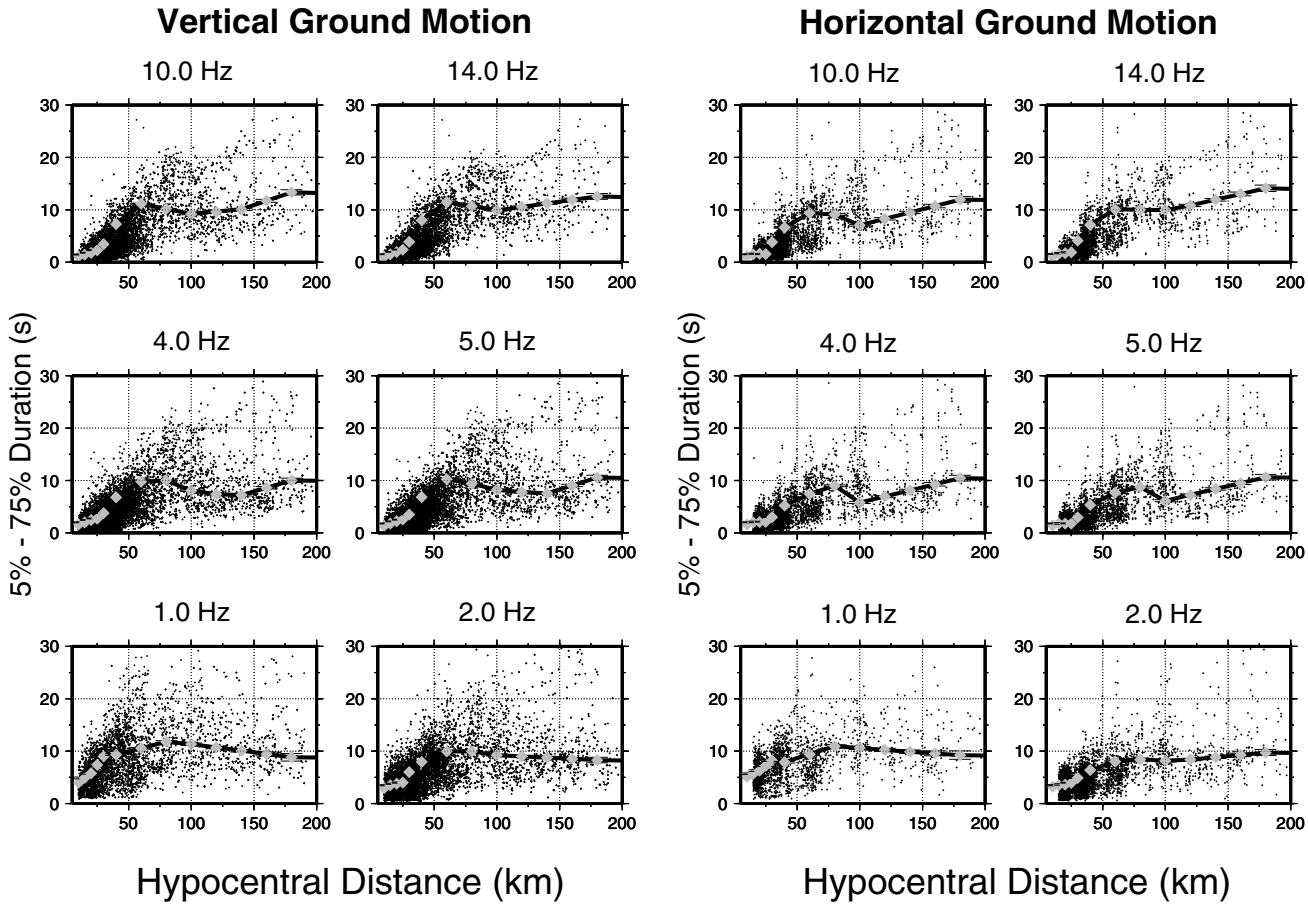

Figure 7. Duration of the ground motion as a function of hypocentral distance at a series of sampling frequencies: the x axes refer to hypocentral distance (km), and the y axes refer to duration (sec). Duration is computed on each individual seismogram in the data set as the time window bracketing the 5%–75% of the integrated seismic energy that follows the S-wave onset (see Fig. 6). Estimates of duration computed on each individual recording are indicated by dark small dots. Large light-gray diamonds linked by piecewise linear curves indicate the L_1-norm estimates of the duration function that were used for RVT predictions of peak amplitudes and response spectra.

We point out that we are able to uniquely define the parameter η in equation (3), which is responsible for the separation of the curves of Figure 8, although a trade-off exists between Q_0 and $g(r)$ at short distances. Some difficulties exist in fitting the high-frequency part of the Fourier spectra, whereas low frequencies are satisfactorily fit. This is probably due to the effect of a higher noise level for the high-frequency Fourier spectra.

Site Terms

Site terms were obtained for the peak filtered velocities and Fourier amplitudes regressions. Plots in Figure 9 show that no peculiar behavior affects the vertical motion of any of the recording sites of the FVGSN, which verifies the accuracy of the instrument calibration.

Constraints were applied to each regression in order to obtain source and propagation terms for the vertical ground motion. The characteristics of the horizontal motion are investigated by analyzing the horizontal site terms or, equivalently, by looking at the horizontal-to-vertical site term ratios, computed at each station where both components of the ground shaking were available. Figure 10 displays the mentioned ratios for both the peak and the Fourier amplitudes; each line in the figure refers to a specific horizontal component, for example, radial and transverse.

It is clear from a visual inspection of Figure 10 that there may be a relation between the H/V ratio and the geologic description given in Table 1. Specifically, site DRE (on marly sandstone and fractured limestone) mimics the generic rock site amplification described by Boore and Joyner (1997). More compact limestone sites (CAE and BAD) are characterized by a lesser amplification at high frequency, whereas a site on dolomite (ZOU) has a horizontal-to-vertical ratio of the site terms essentially flat, and slightly larger than one, over the entire band of interest for this study.

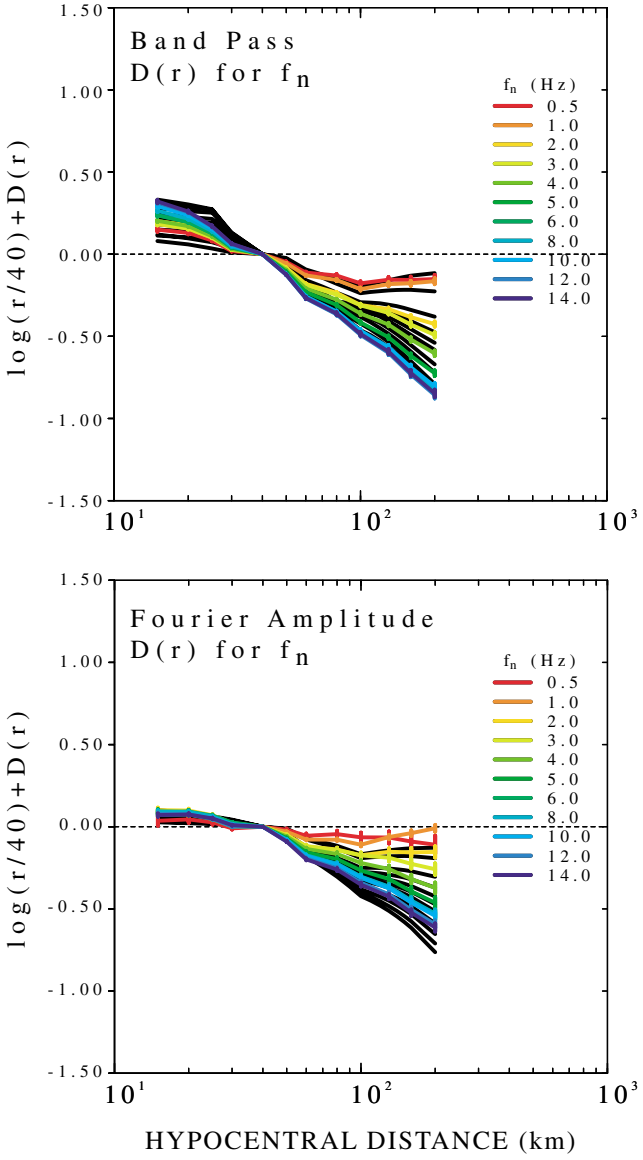

Figure 8. The regional attenuation functional $D(r, r_{ref}, f)$ obtained for the Friuli region from the regressions on the peak amplitudes (color lines, upper frame) and of the Fourier amplitudes (color lines, lower frame) at the sampling frequencies of 0.5, 1.0, 2.0, 3.0, 4.0, 5.0, 6.0, 8.0, 10.0, 12.0, and 14.0 Hz. Both frames refer to vertical ground motion. Attenuation curves has been normalized to zero at a reference hypocentral distance of 40 km and (only for plotting purposes) to a body-wave geometrical attenuation (in other words, the horizontal dashed line plotted in each frame indicates an attenuation $\propto 1/r$). Black lines in the background of each frame indicate theoretical estimates of the regional attenuation, as obtained by using equations (3) to (5) and, for the peak values, by using the tool of RVT, together with the duration estimates of Figure 7. Central frequencies less than 0.5 Hz are not shown in the figure because the relative attenuation curves are not as stable.

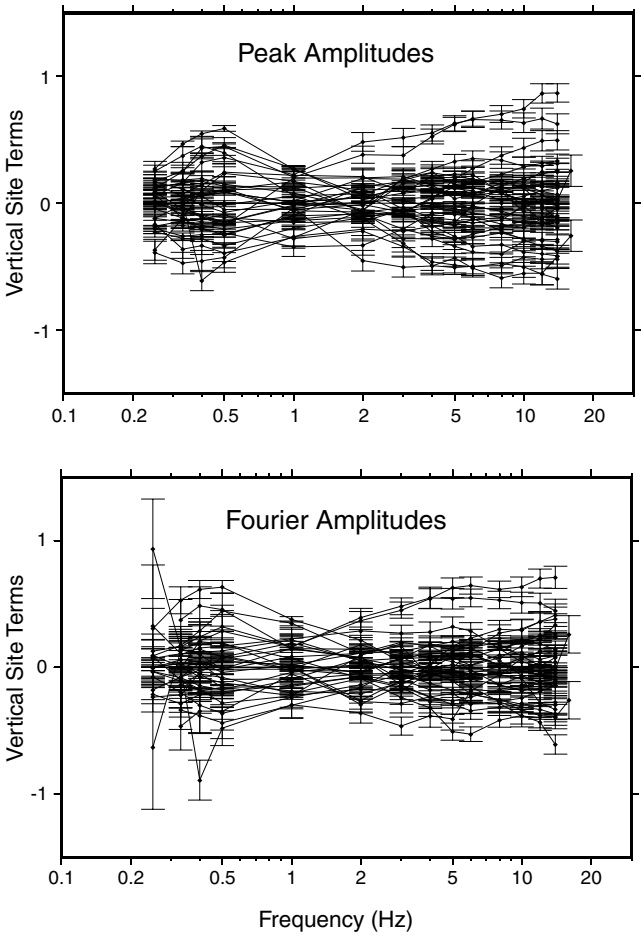

Figure 9. Vertical-component site terms for regressions of peak amplitudes of filtered ground motion (upper) and Fourier amplitudes (lower). The site terms of the both networks are plotted together, but the regressions applied the zero-mean constraints separately to each.

Vertical Excitation Terms

Empirical excitation terms for the vertical ground motion for events of magnitudes M_w 4 and larger are shown in Figure 11 (peak values and Fourier spectra). Excitation terms for the smaller events (although calculated) are omitted in the figure for sake of clarity. These quantities represent the vertical ground shaking as it would be recorded at the reference hypocentral distance, $r_{ref} = 40$ km, by the average network site. Excitation terms ($EXCIT_i$) are related to the predicted level of motion (exc) by: $EXCIT_i = \log 10(\text{exc})$, which is modeled by using the following functional form:

$$\text{exc}(f, r_{ref}) = C(2\pi f) M_0 s(f) g(r_{ref}) \exp\left[-\frac{\pi r_{ref}}{\beta Q_0 (f/f_{ref})^{\eta}}\right] v(f) \exp(-\pi f \kappa_0), \quad (6)$$

where

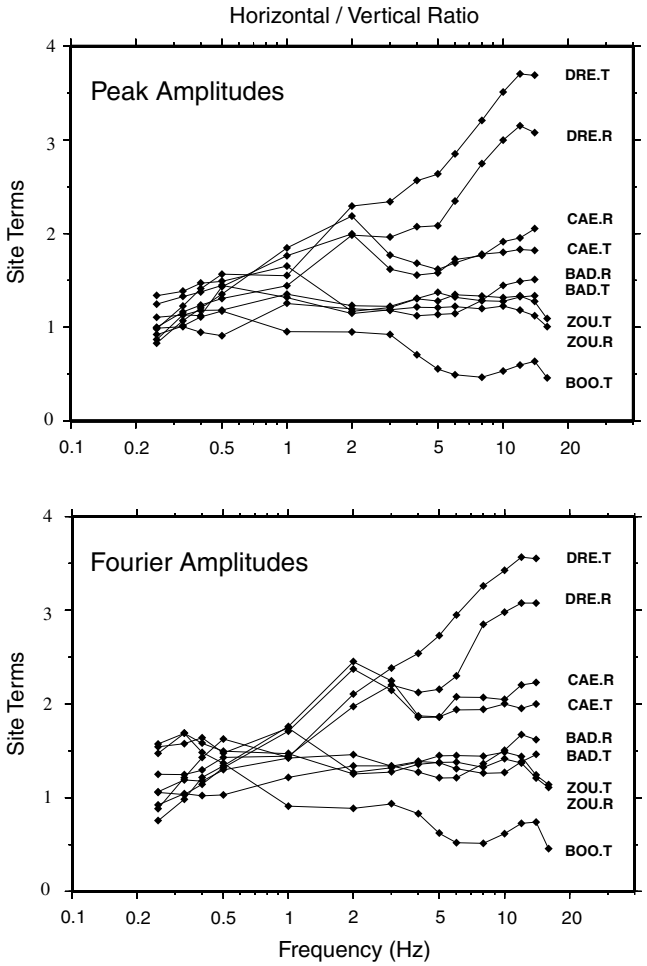

Figure 10. Horizontal-to-vertical ratios for selected stations. This was made possible by applying no constraints on the horizontal site terms. The upper frame of the picture presents the horizontal-to-vertical ratios for the peak amplitude site terms, and the lower frame is for the Fourier amplitude regressions. Site DRE is characterized by a monotonic increase of the horizontal-to-vertical site term ratio with frequency (station on marly sandstone and fractured limestone); sites CAE and BAD (on compact limestone) are characterized by a lesser amplification at high frequency, and site ZOU (on dolomite) is practically flat and close to 1.2 in the entire frequency range.

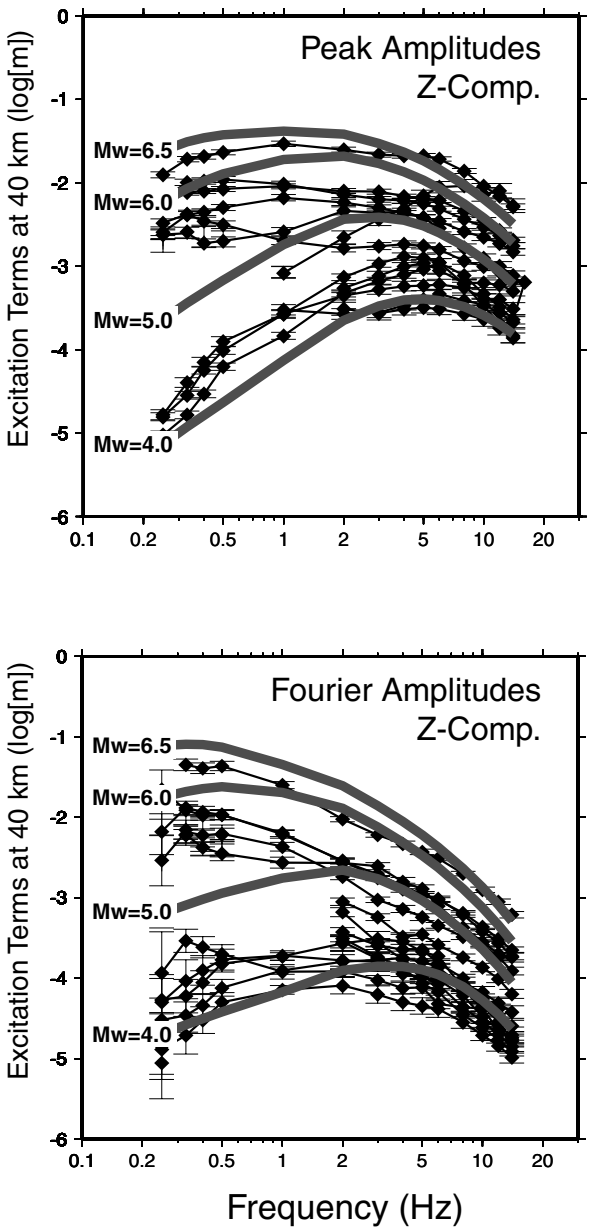

Figure 11. Inverted (black diamonds linked by thin black lines) and theoretical (thick gray lines) excitation terms. The two frames in the figure refer to excitation terms of the vertical motion: peak values are shown in the upper frame, whereas the lower frame is relative to Fourier amplitude spectra. Theoretical quantities relative to vertical-component excitation were obtained by using equations (3) to (9) with the set of parameters listed in Table 3.

$$s(f) = \frac{1 - \epsilon}{1 + (f/f_a)^2} + \frac{\epsilon}{1 + (f/f_b)^2} \qquad (7)$$

and

$$C = (0.55)(0.707)(2.0)/4\pi\rho\beta^3. \qquad (8)$$

$$\kappa_0 = 0.045 \text{ sec} \qquad (9)$$

Here, $v(f)$ is a generic site amplification term (Boore 1986; Atkinson and Silva, 1997; Boore and Joyner, 1997), which in this study is fixed at $v(f) = 1.0$. Our estimate of the high-frequency cutoff parameter in equation (6) is (see Anderson and Hough, 1984); this value was obtained by performing a best fit of the spectra of an average spectral shape using 300 small earthquakes of magnitude $1.8 \leq M_w \leq 2.3$.

De Natale *et al.* (1987) estimated a high-frequency spectral decay function $e^{-\pi\kappa f}$, where $\kappa = 0.06 \pm 0.02$ sec. Due to the short range of travel distances and the scatter of their data, no distance dependence could be estimated by De Natale *et al.* (1987) for κ. Our κ_0 is independent of frequency. Since average effects acting on recording sites are entirely forced on the excitation terms, large anomalies on site behaviors may bias the estimate of κ_0. Recall that, in order to avoid such biases, stations affected by local effects were set free to vary during our regressions. Stations on thin alluvium were not included in the constraint: $\Sigma_i \mathrm{SITE}_i(f) = 0$.

Since the high-frequency level of a small event in the frequency range of 0.25–14 Hz is effectively insensitive to the stress parameter $\Delta\sigma$, the shape is dominated by the effect of the κ_0 parameter of equation (9). The stress parameter $\Delta\sigma$ is defined after κ_0 is quantified by adjusting it to fit the shape of larger events. The small earthquakes essentially are used to define an empirical Green's function for propagation effects.

Since the ENEA-ENEL accelerometric network never overlapped in time with the digital FVGSN, digital and analog recordings were completely decoupled during the regressions. Specifically, the distance terms of Figure 8 were obtained by inverting only the FVGSN digital data and forced to be fixed to these values in a successive inversion carried out only on the ENEA-ENEL strong-motion waveforms.

Because of the nature of the analog accelerometric network that was in use in 1976 and 1977, no small-earthquake recordings were available at these stations to define the κ_0 value independent of the stress parameter. Shaping and amplitudes of the spectra of the largest events were correctly obtained by using the stress parameter indicated in Table 3, an estimate that must be coupled to the value of κ_0 given in equation (9); in addition the stress parameter in Table 3 is biased by the (unknown) frequency-dependent ratio between the average accelerometric network site term and the average FVGSN site term (which we somehow feel not to be far from unity).

To predict the observed high-frequency spectral levels of the largest seismic sources in Figure 11, we used a stress parameter $\Delta\sigma = 60$ MPa. $\Delta\sigma$ is an effective parameter that does not necessarily represent the stress drop relaxed coseismically across the fault plane, but that is needed in order to define, with a single corner frequency Brune spectrum, the spectral shapes and levels of the empirical excitation terms. Nevertheless, Cocco and Rovelli (1989) suggested a stress drop $\Delta\sigma = 30$ MPa for the largest events of the 1976 sequence, whereas a recent study of the source parameters in the Friuli region recently published by Singh *et al.* (2001) also showed that high stress drop parameters (in excess of 100 MPa) are needed in order to reproduce high-frequency spectral levels of earthquakes that occurred in the 8- to 14-km-depth range. The thick gray lines in Figure 11 represent the theoretical excitation terms computed by using equations (4)–(9) at the indicated moment magnitudes. Parameters used to characterize the Brune spectrum are given in Table 3.

Table 3
Parameters of the Spectral Model Used to Compute the Theoretical Excitation Terms of Figure 11

$\rho = 2.8$ g/cm^3
$\beta = 3.5$ km/sec
$\Delta\sigma = 60$ MPa
$f_a = 4.9 \times 10^6 \beta(\Delta\sigma/M_0)^{1/3}$ Hz
$f_b = f_a$
$\varepsilon = 1.0$
$\kappa_0 = 0.045$ sec
$v(f) = 1.0$

De Natale *et al.* (1987) thoroughly studied the source parameters for the 1976–1977 strong-motion records. Their study indicates that relatively high stress drops are needed to model the observed spectra ($\Delta\sigma = 20$–30 MPa). Moreover, time series showed multiple-rupture characteristics, complicating the spectral features of the recordings. Corner frequencies of the largest events seem to be related to subevent ruptures rather than to overall fault size. The presence of an $f_{\max}$ in the range of 5–14 Hz is also indicated by De Natale *et al.* (1987), except for the stations where local site effects produce spectral peaks.

It can also be seen in Figure 11 that the largest events in the data set cannot be modeled perfectly by the use of a single-corner frequency Brune spectral model. This feature is similar to the behavior observed by Mayeda *et al.* (2002) for large earthquakes of the western United States (see also Mayeda and Walter, 1996) and for the Dead Sea Rift and the Gulf of Aqaba; the displacement spectra of these events were clearly characterized by two corner frequencies, by a spectral decay at intermediate frequencies that is between $\omega^{-1.0}$ and $\omega^{-1.5}$, and by a ω^2 rolloff for frequencies above the second corner. The fact that the same behavior of large earthquakes ($M_\omega \geq 6.0$) is observed in very different parts of the world, and, even more importantly, in completely different tectonic environments, makes our observations in the Eastern Alps particularly relevant. Significant departures from an ω^2 source spectrum were also observed in Friuli by Singh *et al.* (2001).

Finally, Figure 12 shows the distributions of the residuals from the regressions (all central frequencies between 0.25 and 14.0 Hz). The residuals from the peak amplitudes (all central frequencies) and high-frequency Fourier spectra ($f_{\mathrm{cl}} \geq 2.0$ Hz) are well behaved, whereas those for the low-frequency Fourier spectra data set (between 0.25 and 1.0 Hz) significantly depart from a Gaussian distribution. The use of an L_1-norm minimization scheme eliminates the effects of non-Gaussian, asymmetric large tails of residuals and the few significant outliers for the high-frequency regressions.

Predicted Ground Motion

The predictive relationships proposed in this study, with the source parameters indicated in Table 3 and the empirical duration function shown in Figure 7, are used to produce the

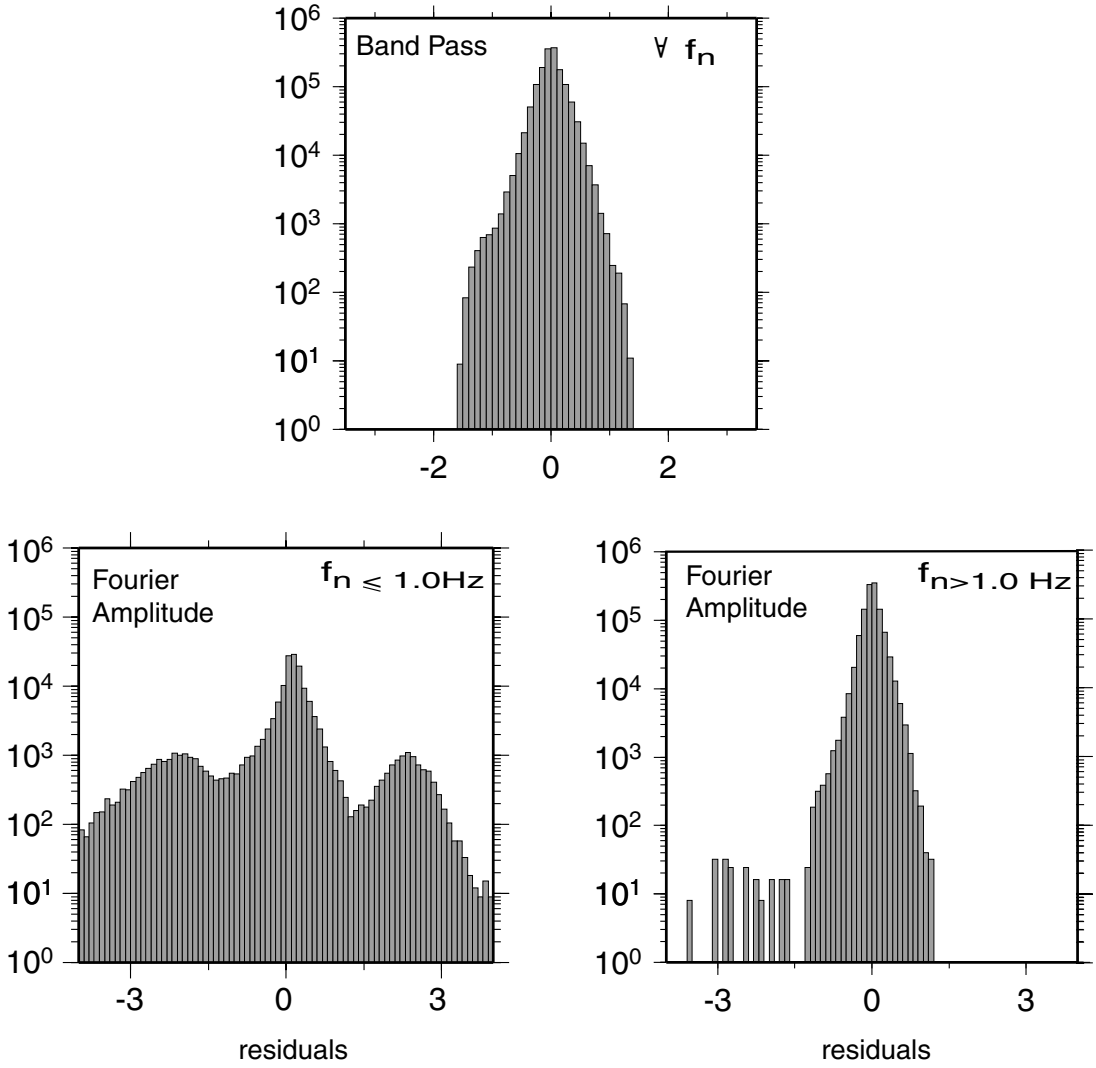

Figure 12. Residuals relative to all sampling frequencies. The upper frame displays a cumulative histogram of all the residuals computed in the regressions of the peak amplitudes (i.e., at all frequencies), whereas residuals computed in the regressions over Fourier amplitudes are separated in two cumulative histograms: central frequencies of 0.25, 0.33, 0.40, and 1.0 Hz (lower left frame), and central frequencies higher than 1.0 Hz (lower right frame). Fourier amplitude residuals are characterized by large outliers at the central frequencies between 0.25 and 1.0 Hz, whereas higher central frequencies are essentially well behaved. Undesirable effects of the non-Gaussian large tails of residuals are eliminated by using an L_1-norm minimization.

theoretical curves of Figures 11 and 8. The ground-motion model (equations 3–9), in the framework of RVT, provides a complete tool for the evaluation of the observed ground-motion characteristics, Fourier spectra, peak filtered velocities, peak velocity, peak acceleration, and response spectra in the entire Friuli region, up to a magnitude level of M_S 6.5 (the largest magnitude ever recorded in the area). In order to evaluate the significance and usefulness of the predictive relationships described in this article, it is important to keep in mind that we have a number of relatively large earthquakes in the data set from the 1976 sequence (M_S 6.5, M_L 6.1, M_L 6.0, M_L 5.9, M_L 5.5, M_S 5.2; see Table 4). The recent event of 12 April 1998, M_w 5.6, was also included in the digital data base.

The chosen model parameters fit the empirical attenuation and excitation functions well for the hypocentral distance, frequency, and magnitude ranges of 20–200 km, 0.25–14 Hz, and between M_w 1.0 and 6.5, respectively. The duration was approximated by a linear function of the hypocentral distance, with zero-intercept and 0.075 sec/km linear coefficient.

The top of Figure 13 compares the results of a theoretical computation of peak horizontal ground acceleration based on the excitation/attenuation parameters estimated in

Table 4
Earthquakes Used for Magnitude Calibration.

Origin Time	Lat. (N)	Long. (E)	Depth (km)	Magnitude
1976 May 06 20:00:13	46.32	13.32	6	M_ω 6.5
1977 Sept 16 23:48:08	46.26	12.98	15	M_S 5.2
1976 Sept 11 16:31:10	46.30	13.23	6	M_L 5.5
1976 Sept 11 16:35:03	46.29	13.18	16	M_L 5.9
1976 Sept 15 03:15:19	46.29	13.20	15	M_L 6.0
1976 Sept 15 09:21:19	46.32	13.16	12	M_L 6.1
1998 Apr 12 10:55:32	46.32	13.67	15	M_w 5.6

Magnitudes of the 1976 events are taken from the Harvard Centroid Moment Tensor (CMT) or the Preliminary Determination of Epicentres Catalog, whereas moment magnitude of the 1998 event is taken from the Harvard CMT catalog.

this study (solid thin lines) to the peak horizontal motions using the relations of Sabetta and Pugliese (1996) (dashed lines) and Ambraseys *et al.* (1996) (dotted lines). We also compare our predictions to values of peak horizontal acceleration observed during the 6 May 1976 M_S 6.5 Friuli earthquake and during two large aftershocks that occurred on 15 September 1976 (M_S ~6.0, 03:15:19 and 09:21:19). Calculations were carried out for M 6.0 and 6.5 through the SMSIM (Boore, 1996). The observed peak horizontal accelerations are very similar to our predictions in the 10- to 100-km distance range, but there are significant differences at larger distances that are mostly due to the presence of alluvium. The bottom of Figure 13 compares our estimates of PGV (solid lines) to those predicted by Sabetta and Pugliese (1996). Due to a higher stability of PGV with respect to PGA, in this case our predictions nicely fit the observations in the entire distance range. To perform both comparisons, epicentral distance was related to hypocentral distances by using a fixed focal depth of 9 km (taken from Cipar, 1980). A recent study by Ambraseys and Douglas (2000) described the results of a regression on a large data set of near-field acceleration time histories. Since the maximum fault distance used in their regression was about 15 km, we were not able to compare our results with theirs.

The choice of magnitude (M_w or M_S) to be used for the theoretical computations of the peak values is problematic because global M_0–M_S conversion relationships (Ekström and Dziewonski, 1988) do not seem to be applicable in Europe (Ambraseys and Bommer, 1991). We used M_w for the numerical computations, and the reader needs to be aware of this issue.

In order to complete the present section, we compared response spectra for 5% damping computed by using the proposed excitation/attenuation model, at magnitudes M 5.0, 6.0, and 7.0 and at the epicentral distances of 15 and 60 km to response spectra obtained from regressions by other authors on strong-motion time histories. Figure 14 presents our response spectra and the ones by the available relationships by Sabetta and Pugliese (1996) (see table 2 of their article) and Ambraseys *et al.* (1996) (from their equation 11 and

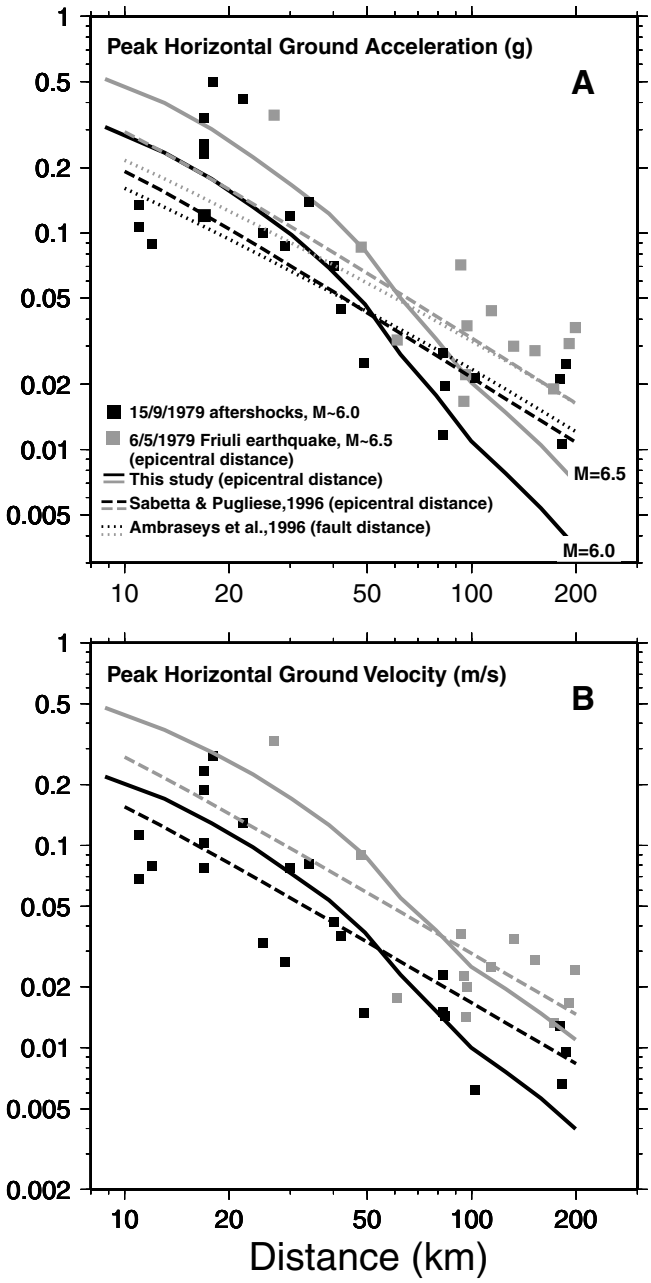

Figure 13. Comparison of different estimates of (A) peak horizontal ground acceleration and (B) peak horizontal ground velocity in Friuli, as obtained by using the empirical relationship by Ambraseys *et al.* (1996) (dotted line), and by Sabetta and Pugliese (1996) (dashed line); solid lines indicate peak horizontal acceleration and velocity computed for hard-rock sites by using Boore's program SMSIM (Boore, 1996), the excitation parameters shown in Table 3, and the crustal attenuation parameters obtained by our trial-and-error modeling of the empirical attenuation functions shown in Figure 8. No generic site amplification function was used. Duration was described by a linear function $T = 0.075r$ (r is the hypocentral distance). Curves are computed for M_w 6.0 and 6.5 and compared to the observed values of peak horizontal acceleration and velocity recorded during the M_w 6.5 earthquake of 6 May 1976 (light solid squares in A and B) and to the ones observed during two aftershocks of M ~6.0 that occurred on 15 September 1976 (dark solid squares in A and B).

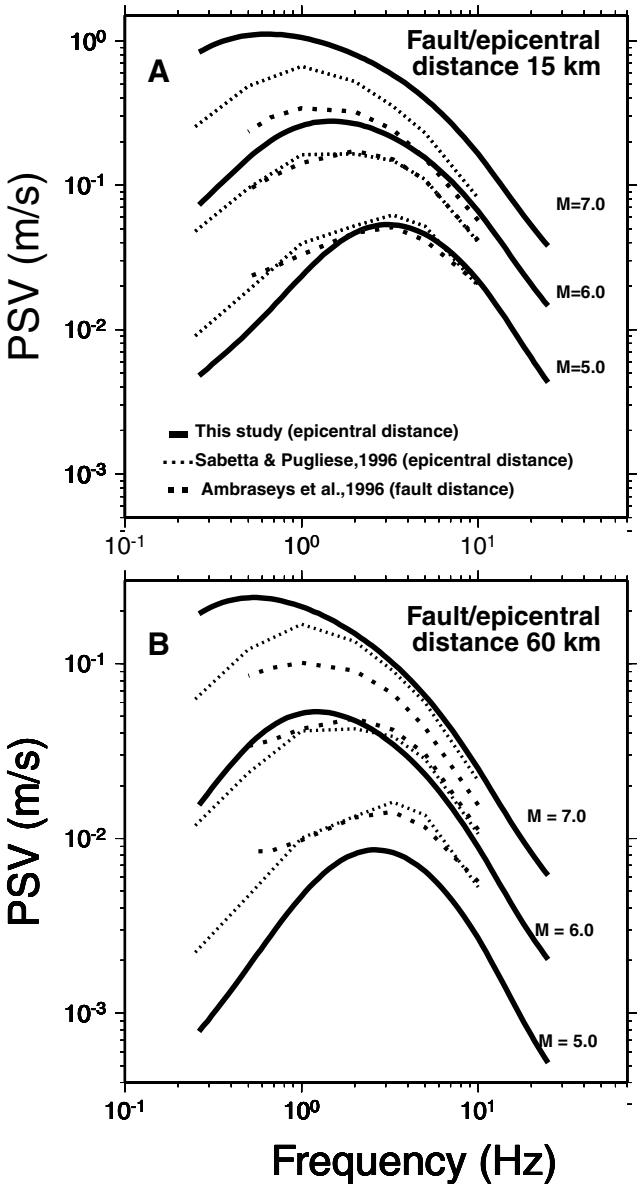

Figure 14. Comparison of horizontal spectra (5% damping) predicted by the ground-motion scaling model presented in this study (solid lines) and the spectral shapes obtained by using the predictive relationships by Ambraseys *et al.* (1996) as a function of frequency and fault distance (dotted lines) and by Sabetta and Pugliese (1996), who performed the regressions also as a function of epicentral distance (dashed lines). (A) rock site, epicentral distance R = 15 km (fault distance is used by Ambraseys *et al.*, [1996]; epicentral distance is used by Sabetta and Pugliese, [1996], as well as in our calculations) and different values of magnitude (M_w 5.0, 6.0, and 7.0). (B) Rock site, M_w 5.0, 6.0, and 7.0 at an epicentral distance of 60 km. Epicentral distance is computed assuming a hypocentral depth of 9 km.

table 1). The 60-km epicentral distance represents the limit of the notable damage ($I \geq 8.5$) suffered in the region during the earthquake of 6 May 1976 (Molin, 2000). Figure 14 compares our results in terms of rock-site spectral response (solid curves) with those of Sabetta and Pugliese (1996) (thick-dashed curves) and by Ambraseys *et al.* (1996) (dotted curves). Parts (A) and (B) of the picture compare, at the epicentral distances of 15 and 60 km, response spectra computed using Boore's program, SMSIM (Boore, 1996), and the set of parameters estimated in this study for the horizontal ground motion (thick solid lines) to empirical estimates by Ambraseys *et al.* (1996) (dotted lines) and by Sabetta and Pugliese (1996) (dashed lines).

Hypocentral distances in our computation have been transformed in epicentral distances for use in Figure 14 by assuming a source depth of 9 km. In numerous studies, people have used the distance from the fault (the closest distance from the surface projection of the fault): epicentral and fault distances essentially coincide at larger distances. Even if this approximation may get very weak for large events, we assume that it is an acceptable compromise for the purpose of mere comparison with other authors' results. Comparing our results with those by Sabetta and Pugliese (1996), whose table 2 refers to epicentral distance, and by Ambraseys *et al.* (1996), who used fault distance instead, we observe that, at an epicentral (or fault) distance of 15 km and for M 6.0, the different curves are close to each other. Moreover, at all frequencies and at an epicentral (fault) distance of 15 km, predictions from this study are the highest for M 7.0 and the lowest for M 5.0. On the other hand, at an epicentral distance of 60 km, except at low frequencies, our results are very close to the ones by Sabetta and Pugliese (1996) and by Ambraseys *et al.* (1996) at M 7.0. It is important to mention that Ambraseys *et al.* (1996) gave their results in terms of fault distance. At lower magnitudes, the three curves essentially coincide for M 6, whereas at M 5, our predicted velocity response spectrum is substantially lower than the other two.

Finally, in order to provide information about distance scaling of the response spectra, in Figure 15 we provide the horizontal response spectra (pseudovelocity, 5% damping) predicted for an M_w 6.0 event by the ground-motion scaling model presented in this study at different hypocentral distances. Spectra are provided every 10 km; thick lines are used to highlight theoretical response spectra at 10, 50, and 100 km from the hypocenter.

Discussion

A number of recent studies cited in this article have shown that differences in the attenuation characteristics of the crust between areas characterized by different tectonic regimes and thermal ages may significantly bias the hazard estimates if the predictive relationships for the ground motion are computed over data sets of heterogeneous nature. In this respect, regional studies that have been systematically

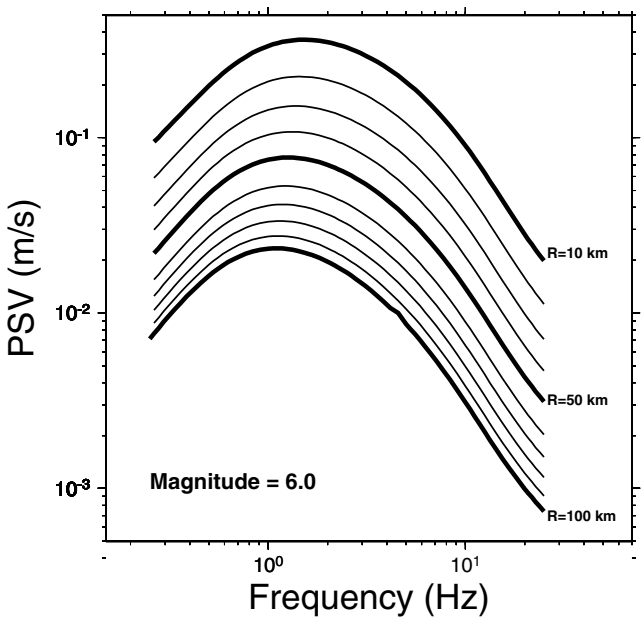

Figure 15. Prediction of horizontal response spectra (5% damping) for an M_w 6.0 event for northeastern Italy at different hypocentral distances. Spectra are provided every 10 km for a rock site; thick lines are used to plot spectra at 10, 50, and 100 km from the hypocenter.

carrying out by our working group (INGV–Sezione, Sismologia e Sismotettonica, Unità di Progetto Pericolosità Sismica, and Project Ground-Motion Scaling in the Mediterranean Region) over-the entire Mediterranean area and over the rest of Europe as well, have the ultimate goal of producing an Euro-Mediterranean hazard map where the predictive relationships used to describe the excitation and the attenuation of the ground motion are calibrated at the regional scale.

The goal of the present study is to provide the seismological and engineering communities with an empirical tool for the prediction of the ground motion in the Eastern Alps. The tool consists of two main parts. The first one quantifies the crustal attenuation, whereas the second one represents an effective source model for the region. Although the two parts are strictly decoupled by the set of constraints forced on the systems before the regressions, they both contains parameters that may severely trade off with one another. This section of the article is devoted to the discussion of the physical meaning of the quantities given in this article.

This study substantially improves the estimate of the frequency-dependent crustal attenuation parameter for the region over that previously available. Console and Rovelli (1981), by using strong-motion acceleration spectra from the two strongest events occurred in 1976 (May and September), estimated

$$Q(f) = 80f^{1.1} \tag{10}$$

in the 0.1- to 10.0-Hz frequency band. They also found a strong frequency dependence for the crustal attenuation parameter $Q(f)$, increasing from $Q(f = 1.0\ \text{Hz}) = 50$–$200$ to $Q(f = 20\ \text{Hz}) = 1000$–$2000$.

The frequency dependence suggested by Console and Rovelli (1981) seems to be extremely high when compared with other results from adjacent regions. In fact, Malagnini *et al.* (2000a) and Malagnini and Herrmann (2000) observed

$$Q(f) = 130f^{0.10} \tag{11}$$

in the Apennines. Moreover, Malagnini *et al.* (2000b) computed $Q(f) = 400f^{0.42}$ in Central Europe, Bay *et al.* (2001) found $Q(f) = 490f^{0.35}$ in Switzerland, and Morasca *et al.* computed $Q(f) = 310f^{0.20}$ for the western Italian Alps. The frequency dependence is also very high if we compare it with results from other regions of the world: Raoof *et al.* (1999) suggested $Q(f) = 180f^{0.42}$ for crustal attenuation in southern California; Jeon (2000) estimated it to be between $Q(f) = 145f^{0.65}$ and $Q(f) = 180f^{0.60}$ for Utah (Basin and Range Province).

It is clear that the steepness of the geometrical decay trades off with the anelastic parameter Q_0 in equation (3). On the contrary, the effect of the exponent η in equation (3) (Fig. 8) is completely decoupled from the other high-frequency parameter, κ_0 in equation (6), by the normalization constraint $D(r = r_{\text{ref}}, f) = 0$. The effect of κ_0 on the regional attenuation function shown in Figure 8 is completely removed by the normalization of the propagation term, and it is forced entirely over the excitation terms plotted in Figure 11. Also, the fact that a single value for Q_0 is used at all distances is somehow inappropriate because the direct radiation recorded at short distances mainly samples the crust above the hypocenter, whereas at large distances the seismic waves sample the entire crust. Finally, it is important to understand that the method used in this article completely loses the azimuthal or depth information contained in each recording, giving a somehow crude picture of the statistical characteristics of the crustal-wave propagation in the region.

Many of the existing predictive relationships for the Italian and European regions (e.g., Ambraseys and Bommer, 1991, Ambraseys, 1995, Ambraseys and Simpson, 1996; Ambraseys *et al.*, 1996; Sabetta and Pugliese, 1987, 1996) were obtained by forcing a body-wave geometrical spreading to a distance range where supercritical reflections at the Moho appear to be of fundamental importance; this was done because the distance distribution of the observations did not allow more detailed analyses of the characteristics of the geometrical spreading. On the other hand, our data set was very large, allowing the investigation of details in the crustal propagation in northeastern Italy.

A more complex argument is needed to completely understand the nature of the excitation model, for it involves the use of the stress drop parameter, $\Delta\sigma$, whose physical meaning may be severely misunderstood if the coupling

(trade-off) with other parameters (such as κ_0 or the generic rock amplification factor $v(f)$ of Table 3) is not completely clear. In our study, κ_0 represents a regional average of the effective anelastic attenuation at shallow depth, averaged over all the sites that were used in the null-summation constraint.

Regarding the physical meaning of the stress parameter at the largest magnitudes, recall that those earthquakes occurred in 1976–1977 and were recorded by an analog accelerometric network that never overlapped in time with the FVGSN. For this reason, the digital and analog recordings were completely decoupled during the regressions. Moreover, since no small-earthquake recordings were ever recorded by the accelerometric stations, the estimate of κ_0 indicated in equation (9) strictly and only refers to the average between the sites monitored by the FVGSN. The choice of using the same value of κ_0 in order to model the excitation terms of the events recorded by the analog network was completely arbitrary, and so the empirical estimate of the stress parameter given in Table 3 must always be coupled to the value of κ_0 indicated in equation (9). That estimate is also biased by the (unknown) frequency-dependent ratio between the average accelerometric network site term and the average FVGSN site term.

Systematic site effects acting on every station of the network are entirely transferred on the excitation terms; in this respect, it may be appropriate to model the empirical excitation terms by multiplying the Brune spectral model by a suitable amplification function, $v(f)$ (Boore, 1986; Atkinson and Silva, 1997). We chose to force $v(f) = 1.0$ in equation (6) (see Table 3), and it should be clear that the implication of this choice is that the stress parameter indicated in this article for the Friuli region ($\Delta\sigma = 60$ MPa) is inherently an "apparent" parameter and should not be understood as the amount of stress that was actually relaxed across the fault surface during the largest earthquakes of the 1976 sequence. It is necessary to keep in mind that the entire predictive relationship proposed in this study (including the empirical duration function of Fig. 7) represents no more than an empirical tool to predict the ground motion anywhere in the region; on the other hand, the crustal attenuation function may be used to properly deconvolve the propagation effects (including κ_0) from the seismic recordings in order to fully isolate the source spectrum for further studies.

Our estimate of the anelastic parameter κ_0 is obtained in a perfectly linear regime, whereas Atkinson and Silva (1997) showed that κ may be magnitude dependent (beyond a certain threshold, κ positively correlates with magnitude, a clear symptom of nonlinear behavior). We compare the expected PGA and PGV response spectra (5% damping) to the predictions by Ambraseys *et al.* (1996) and by Sabetta and Pugliese (1996). Predicted peak values based on our excitation/attenuation model agree well with the empirical results of the mentioned authors and with observed peak values as well. Although the predictive relationships presented here are to be used to compute the ground motion in a wide magnitude range, we must keep in mind that all the calculations are performed for rock sites and that nonlinearities may play an important role at some specific sites, decreasing peaks and Fourier amplitudes of the ground motion excited during moderate and large events.

Conclusions

We investigated the ground-motion scaling in the region monitored by the FVGSN in northeastern Italy. A tremendous amount of data (a total of 17,238 seismograms: 10,256 vertical and 6982 horizontal) was used in our regressions to obtain the excitation and attenuation of bandpass-filtered PGVs and of Fourier amplitude spectra. The analyses were performed in the frequency range between 0.25 and 14.0 Hz, up to the highest magnitude level ever recorded in the region—the event that occurred on 6 May 1976 at 20:00 local time (M_s 6.5), making the results of this study particularly valuable for structural engineering purposes. Other than the event just mentioned, data from six other earthquakes of substantial sizes ($M \geq 5.2$), (three having $M \sim 6$), were included in the database.

Given a source spectral model, the attenuation model for the region, and an empirical function to describe the dispersion-induced duration of the ground motion as a function of hypocentral distance and frequency, RVT was used with a single-corner frequency spectral model (Brune, 1970, 1971) to model the absolute level of ground shaking. To accomplish this, it was necessary to use a stress drop parameter $\Delta\sigma = 60$ MPa, one much larger than that obtained by Cocco and Rovelli (1989), together with the high-frequency rolloff controlled by $\exp(-\pi\kappa_0 f)$, $\kappa_0 = 0.045$ sec. Of course, the use of a single estimate of stress drop for over the largest events of 1976 may represent a limitation of the presented results. In fact, recent works have pointed out that the stress parameter may significantly vary with the earthquake magnitude (e.g., Mayeda and Walter, 1996), although it is clear that, in the frequency range of engineering and seismological interest, the spectral levels of the largest events are more sensitive to stress drop than those of the small events.

The use of a single-corner frequency Brune spectrum model does not fit the large earthquake data perfectly. This behavior has been previously observed for large events in different regions of the world—see the article on the western United States by Mayeda and Walter (1996) and on the Dead Sea Rift and Gulf of Aqaba by Mayeda *et al.* (2002)—and might represent a general feature of nonsubduction events of M <6.5. A spectral model characterized by two corner frequencies would probably better describe the observed excitation terms for large events in Friuli, substantially changing the amount of radiated energy at intermediate frequencies. The use of such a model may significantly impact the estimates of seismic hazard in the region. Of course, the present study does not focus on this issue because of its

emphasis on defining the distance dependence of high-frequency motion in the region.

Differences are seen in the geometrical spreading functions at low and high frequencies: a laminated lower crust, for example, a thick crust–mantle transition zone, might be responsible for this behavior. For the crustal anelasticity in the region, the following parameter is suggested:

$$Q(f) = 260\left(\frac{f}{f_{\text{ref}}}\right)^{0.55}; f_{\text{ref}} = 1.0 \text{ Hz}. \qquad (12)$$

This and related studies (Malagnini and Herrmann, 2000; Malagnini *et al.* 2000a) demonstrated that important variations of the attenuation parameters take place within the Italian region. Results of this study may be extrapolated to $M_w > 6.5$ within the investigated region with extreme caution, and it is important to point out that comparisons with the observations of peak ground-motion amplitudes collected for large earthquakes in Italy ($M \sim 7$) rely only on recordings of the 1980 Irpinia earthquake, ($M \sim 7$) in the southern Apennines.

Acknowledgments

The authors wish to thank Alberto Michelini and Pierluigi Bragato from OGS, Trieste, for kindly and promptly providing data. This study was supported by the Gruppo Nazionale Difesa dai Terremoti, (GNDT) through the project Terremoti probabili in Italia tra l'anno 2000 e il 2030: elementi per la definizione di priorità degli interventi di riduzione del rischio sismico, task 3.1. The contribution of R. B. Herrmann was supported in part by the Earthquake Engineering Research Center's Program of the National Science Foundation under Award No. EEC-9701785.

References

Akinci, A., L. Malagnini, N. A. Pino, L. Scognamiglio, R. B. Herrmann and H. Eyidogan (2001). High-frequency ground motion in the Erzincan region, Turkey: inferences from small earthquakes, *Bull. Seism. Soc. Am.* **91,** 1446–1455.

Ambraseys, N. N. (1995). The prediction of earthquake peak ground acceleration in Europe, Earthquake *Eng. Struct. Dyn.* **24,** 467–490.

Ambraseys, N. N., and J. J. Bommer (1991). The attenuation of ground acceleration in Europe, *Earthquake Eng. Struct. Dyn.* **20,** 1179–1202.

Ambraseys, N. N., and J. Douglas (2000). Reappraisal of the effect of vertical ground motions on response, ESEE Report No. 00-4, August 2000, Engineering Seismology and Earthquake Engineering, 60 pp.

Ambraseys, N. N., and K. A. Simpson (1996). Prediction of vertical response spectra in Europe, *Earthquake Eng. Struct. Dyn.* **25,** 401–412.

Ambraseys, N. N., K. A. Simpson, and J. J. Bommer (1996). Prediction of horizontal response spectra in Europe, *Earthquake Eng. Struct. Dyn.* **25,** 371–400.

Anderson, J. G., and S. E. Hough (1984). A model for the shape of the Fourier amplitude spectrum of acceleration at high frequencies, *Bull. Seism. Soc. Am.* **74,** 1969–1993.

Aric, K., R. Gutdeutsch, G. Klinger, and W. Lenhardt (1987). Seismological studies in the Eastern Alps, in *Geodynamics of the Eastern Alps*, H. W. Fluegel and P. Faupl (Editors), Franz Deuticke, Vienna, Austria, 325–333.

Atkinson, G. M., and W. Silva (1997). An empirical study on earthquake source spectra, *Bull. Seism. Soc. Am.* **87,** 97–113.

Bartels, R. H., and A. R. Conn (1980). Overdetermined systems of linear equations in the L1 sense, with or without linear constraints, *ACM TOMS* **6,** 609–614.

Bay, F., D. Fäh, L. Malagnini, and D. Giardini (2003). Spectral shear-wave ground motion scaling for Switzerland, *Bull. Seism. Soc. Am.* (in press).

Bonamassa, O., and A. Rovelli (1986). On distance dependence of local magnitudes found from Italian strong-motion accelerograms, *Bull. Seism. Soc. Am.* **76,** 579–581.

Boore, D. M. (1986). Short-period *P*- and *S*-wave radiation from large earthquakes: implication for spectral scaling relations, *Bull. Seism. Soc. Am.* **76,** 43–64.

Boore, D. M. (1996). SMSIM: Fortran programs for simulating ground motion from earthquakes, version 1.0, *U.S. Geol. Surv. Open-File Report 96-80-A*, 73 pp.

Boore, D. M., and W. B. Joyner (1997). Site amplification for generic rock sites, *Bull. Seism. Soc. Am.*, **87,** 327–341.

Boore, D. M., W. B. Joyner, and T. E. Fumal (1993). Estimation of response spectra and peak acceleration from western North America earthquakes: an interim report, *U.S. Geol. Surv. Open-File Rept. 93-509*, 72 pp.

Braitenberg, C. (2000). Non-random spectral components in the seismicity of NE Italy, *Earth Planet. Sci. Lett.* **179,** 379–390.

Bressan G., A. Snidarcig, and C. Venturini (1998). Present state of tectonic stress of the Friuli area (eastern Southern Alps), *Tectonophysics* **292,** 211–227.

Brune, J. N. (1970). Tectonic stress and the spectra of seismic shear waves from earthquakes, *J. Geophys. Res.* **75,** 4997–5009.

Brune, J. N. (1971). Correction, *J. Geophys. Res.* **76,** 5002.

Campbell, K. W., and Y. Bozorgnia (1994). Near-source attenuation of peak horizontal acceleration from worldwide accelerograms recorded from 1957 to 1993, in *Proc. Fifth U.S. National Conference on Earthquake Engineering*, EERI, Berkeley, California, Vol. 1, 283–292.

Carulli G. B., R. Nicolich, A. Rebez, and D. Slejko (1990). Seismotectonic of the Northwest External Dinarides, *Tectonophysics* **179,** 11–25.

Cartwright, D. E., and M. S. Longuet-Higgins (1956). The statistical distribution of the maxima of a random function, *Proc. R. Soc. London* **A237,** 212–232.

Chiaruttini, C., and L. Siro (1981). The correlation of peak ground horizontal acceleration with magnitude, distance, and seismic intensity for Friuli and Ancona, Italy, and the Alpide Belt, *Bull. Seism. Soc. Am.* **71,** 1993–2009.

Chouet, B., K. Aki, and M. Tsujiura (1978). Regional variation of the scaling law of earthquake source spectra, *Bull. Seism. Soc. Am.* **68,** 49–79.

Cipar, J. (1980). Teleseismic observations of the 1976 Friuli, Italy, earthquake sequence, *Bull. Seism. Soc. Am.* **70,** 963–983.

Cocco, M., and A. Rovelli (1989). Evidence for the variation of stress drop between normal and thrust faulting earthquakes in Italy, *J. Geophys. Res.* **94,** 9399–9416.

Console, R., and A. Rovelli (1981). Attenuation parameters for Friuli region from strong-motion accelerogram spectra, *Bull. Seism. Soc. Am.* **71,** 1981–1991.

Cramer, C. H., and J. S. Gomberg (2001). Updated New Madrid analysis better defines the uncertainty in seismic hazard maps, *EOS* **82,** no. 102, 106.

De Natale, G., R. Madariaga, R. Scarpa, and A. Zollo (1987). Source parameters analysis from strong motion records of the Friuli, Italy, earthquake sequence (1976–1977), *Bull. Seism. Soc. Am.* **77,** 1127–1146.

Ekström, G., and A. Dziewonski (1998). Evidence of bias in estimation of earthquake size, *Nature* **332,** 319–323.

Gebrande, H., H. Haege, G. H. Miller, G. Mueller, and E. Schmedes (1978). Aftershock investigations and fault-plane solutions of the Friuli earthquakes 1976, in *Alps, Apennines, Hellenides*, H. Closs, D. Roeder, and K. Schmidt (Editors), Inter-Union Commission on Geodynamics Scientific Report 38. E. Schweizerbart'sche Verlagsbuchhandlung, Stuttgart, Germany, 173–177.

Giese, P., and C. Prodehl (1976). Main features of crustal structure in the

Alps, in *Explosion Seismology in Central Europe: Data and Results*, P. Giese, C. Prodehl, and A. Stein (Editors), Springer-Verlag, Berlin, Germany, Vol. 1, 347–375.

Herrmann, R. B., and J. Dutt (1999). High frequency vertical ground motion in the Pacific Northwest using PNSN data, *Seism. Res. Lett.* **70,** 216.

Herrmann, R. B., and L. Malagnini (1996). Absolute ground motion scaling in the New Madrid Seismic Zone, *Seism. Res. Lett.* **67,** 40.

Istituto Nazionale di Oceanografia e Geofisica Sperimentale (OGS) (2000). *Bollettino della Rete Sismometrica del Friuli-Venezia Giulia*, Centrodi Recerche Sismologiche, Udine, Vol. 8, September 2000, 29 pp.

Jeon, Y.-S. (2000). High-frequency earthquake ground motion scaling in Utah, *Master Thesis*, Saint Louis University, 106 pp.

Kramer, S. L. (1996). *Geotechnical Earthquake Engineering*, International Series in Civil Engineering and Engineering Mechanics, Prentice Hall, Upper Saddle River, New Jersey, 653 pp.

Malagnini, L., and R. B. Herrmann (2000). Ground motion scaling in the region of the Umbria-Marche earthquake of 1997, *Bull. Seism. Soc. Am.* **90,** 1041–1051.

Malagnini, L., R. B. Herrmann, and M. Di Bona (2000a). Ground motion scaling in the Apennines (Italy), *Bull. Seism. Soc. Am.* **90,** 1062–1081.

Malagnini, L., R. B. Herrmann, and K. Koch (2000b). Regional ground motion scaling in Central Europe, *Bull. Seism. Soc. Am.* **90,** 1052–1061.

Mayeda, K., and W. R. Walter (1996). Moment, energy, stress drop, and source spectra of western United States earthquakes from regional coda envelopes, *J. Geophys. Res.* **101,** 11,195–11,208.

Mayeda, K., A. Hofstetter, J. L. O'Boyle and W. R. Walter (2002). Stable and transportable regional magnitudes based on coda-derived moment-rate spectra, *Bull. Seism. Soc. Am.* (submitted).

Molin, D. (2000). Terremoto del Friuli del 6 maggio 1976: Caratteri macrosismici, in *Itinerario nel 1976: Viaggio nella storia sismica del Friuli*, L. Peruzza, D. Slejko, and M. Riuscetti (Editors), Trieste, Italy. (CD-ROM).

Morasca, P., L. Malagnini, A. Akinci, and D. Spallarossa (2002). Ground-motion scaling in the Western Alps, *Seism. Res. Lett.* **13,** 251.

Newmark, N. M., and W. J. Hall (1982). *Earthquake Spectra and Design*, Earthquake Engineering Research Institute, Berkeley, 103 pp.

Ortega, R., and R. B. Herrmann (2000). High-frequency ground motion in Central Mexico: site, excitation and attenuation, *Seism. Res. Lett.* **71,** 246.

Pino, N. A., L. Malagnini, A. Akinci, L. Scognamiglio, R. B. Herrmann, G. Stavrakakis, and G. Chouliaras (2001). Ground motion scaling relationships for mainland Greece and Crete, *Seism. Res. Lett.* **72,** 258.

Pondrelli, S., G. Ekström, and A. Morelli (2001). Seismotectonic re-evaluation of the 1976 Friuli, Italy, seismic sequence, *J. Seismology* **5,** 73–83.

Raoof, M., R. B. Herrmann, and L. Malagnini (1999). Attenuation and excitation of three-component ground motion in Southern California, *Bull. Seism. Soc. Am.* **89,** 888–902.

Sabetta, F., and A. Pugliese (1987). Attenuation of peak horizontal acceleration and velocity from Italian strong-motion records, *Bull. Seism. Soc. Am.* **77,** 1491–1511.

Sabetta, F., and A. Pugliese (1996). Estimation of response spectra and simulation of nonstationary earthquake ground motion, *Bull. Seism. Soc. Am.* **86,** 337–352.

Samiezade-Yazd, M. R. (1993). Ground motion studies in the Southern Great Basin of Nevada and California, *Ph.D. Thesis*, Saint Louis University, 203 pp.

Scognamiglio, L., L. Malagnini, A. Akinci, G. Di Grazia, N. A. Pino, and A. Ursino (2001). Ground motion scaling in the Eastern Sicily, *EOS* **82,** no. 47 (fall meeting suppl.), abstract S4C-0606.

Selli, R. (1963). Schema geologico delle Alpi Carniche e Giulie Occidentali, *Giornale di Geologica* **30,** 1–136.

Singh, D. D., A. Govoni, and P. L. Bragato (2001). Coda Q_c attenuation and source parameter analysis in Friuli (NE Italy) and its vicinity, *Pure Appl. Geophys.* **158,** 1737–1761.

Slejko, D. (1987). Modello sismotettonico del Friuli, scuotibilita' e rischio sismico, in *Aree sismogenetiche e rischio sismico in Italia*, E. Boschi and M. Dragoni (Editors), Editrice Galileo Galilei, Lausanne, Vol. 1, 327–370.

Slejko D., G. B. Carulli, R. Nicolich, A. Zanferrari, A. Cavallin, C. Doglioni, F. Carraro, D. Castaldini, V. Iliceto, E. Semenza, and C. Zanolla (1989). Seismotectonics of the eastern southern-Alps: a review, *Boll. Geof. Teor. Appl.* **31,** 109–135.

Spalletta, C., and C. Venturini (1989). Stratigraphic correlation of the Paleozoic Sequenze in the Carnic Alps (Italy), *Rend. Soc. Geol. Ital.* **12,** 417–421.

Istituto Nazionale di Geofisica e Vulcanologia
Rome, Italy
(L.M., A.A., N.A.P., L.S.)

Department of Earth and Atmospheric Sciences
Saint Louis University, St. Louis, Missouri
(R.B.H.)

Manuscript received 27 July 2001.